THE ASTROPHYSICAL JOURNAL, 413:641–657, 1993 August 20

EVOLUTION OF LOW- AND INTERMEDIATE-MASS STARS TO THE END OF THE ASYMPTOTIC GIANT BRANCH WITH MASS LOSS

E. VASSILIADIS[1,2] AND P. R. WOOD[1]
Received 1992 October 22; accepted 1993 February 24

ABSTRACT

Stars with initial masses in the range $0.89 \leq M/M_{\odot} \leq 5.0$ have been evolved from the main-sequence phase through to the end of the asymptotic giant branch (AGB). The calculations were done with metallicities Z of 0.016, 0.008, 0.004, and 0.001 to allow comparison with Galactic and Magellanic Cloud stars. The novel feature of these calculations is the inclusion of mass loss on the AGB using an empirical formula relating the mass-loss rate to the pulsation period. The calculations show that a *superwind* phase develops naturally on the AGB, but only over the last 2–3 thermal pulse cycles. Since the superwind operates only during the latter part of the quiescent (hydrogen burning) phases when the luminosity is high, most AGB stars probably experience several superwind phases between which the star would appear as a normal optically visible red giant. Estimates are made, as a function of mass and metallicity, for the lifetimes of the thermally pulsing AGB phase, the optically visible AGB phase, and the maximum pulsation periods for OH/IR and other pulsating dust-enshrouded AGB stars. The maximum AGB luminosities predicted from this work for stars with initial masses $\lesssim 3\ M_{\odot}$ are in excellent agreement with those observed for stars in Magellanic Cloud clusters. It is argued that current observational estimates of maximum AGB luminosities for more massive cluster stars are too faint. The initial-final mass relation should therefore be reliable, at least for initial masses $\lesssim 3\ M_{\odot}$, although it predicts white dwarf masses $\sim 0.1\ M_{\odot}$ larger than the current observational calibration of the relation. In the stars of initial mass $5.0\ M_{\odot}$, helium shell flashes are found to be weak, and the evolutionary tracks are overluminous with respect to the classical AGB luminosity-core mass relation provided the envelope mass is large ($\gtrsim 1.5\ M_{\odot}$). Such stars evolve *down* the AGB as envelope mass is reduced during the superwind phase. Finally, we note that the calculations fail to reproduce the high frequency of low-mass carbon stars which is observed in the Magellanic Clouds, a failure evident in other computations of AGB evolution.

Subject headings: stars: AGB and post-AGB — stars: evolution — stars: interiors — stars: mass-loss

1. INTRODUCTION

Two essential features of asymptotic giant branch (AGB) evolution are thermal pulses (also called helium shell flashes) and mass loss. Direct evidence for the occurrence of thermal pulses is provided by the rapid observed period changes in some Mira variables (Wood & Zarro 1981). Thermal pulses also give rise to red giants such as the S and C stars in which the surface abundances have clearly been modified by contamination with nuclear processed material from the interior (Iben 1975).

The importance of mass loss is demonstrated by the fact that the progeny of AGB stars, the planetary nebula nuclei (PNNs) and white dwarfs, have mass distributions peaked closely around $0.6\ M_{\odot}$ (Weidemann & Koester 1983; Weidemann 1990) while the main-sequence masses of these objects must have been $\gtrsim 1\ M_{\odot}$ (Pottasch 1984; Jura 1990). It is also clear that the mass loss between the main sequence and the white dwarf stage occurred largely on the AGB. Working back from the planetary nebula (PN) phase, the typical PN mass of $\sim 0.2\ M_{\odot}$ means that this amount of mass was ejected on the AGB. Renzini (1981) noted that the mean mass-loss rate required in order to produce the typical PN was $\sim 3 \times 10^{-5}\ M_{\odot}\ \mathrm{yr}^{-1}$, and he introduced the term *superwind* to describe such mass-loss rates since they are much higher than the rates given by the widely used mass-loss formula of Reimers (1975). Since that time, many AGB stars (particularly infrared sources, OH/IR stars, and Mira variables) have been found to have mass-loss rates consistent with the superwind values (e.g., Knapp & Morris 1985 in the Galaxy, and Wood et al 1992 in the LMC). The frequent occurrence of such objects means that the production of planetary nebulae (PNs) by discrete ejection events such as dynamical instability of the envelope (Roxburgh 1967; Paczyński & Ziolkowski 1968) is unlikely. However, the interaction of mass-loss mechanisms with the changes in surface luminosity produced by helium shell flash cycles should still modulate the mass-loss rate. It is the interplay between mass loss and evolution on the AGB that this paper sets out to address.

Few of the previous stellar evolution calculations of AGB evolution have included mass loss, and when this has been done (Schönberner 1979, 1981, 1983; Boothroyd & Sackmann 1988a–d), the mass loss has been incorporated in the form defined by Reimers (1975). As noted above (see also Iben & Renzini 1983; Wood 1986), this formula fails to produce mass loss at anything like the rates observed in AGB stars. In this paper, empirical data based on observations of AGB stars are used in order to derive the mass-loss rate.

Given a reliable estimate of the mass-loss rate for AGB stars, the study of AGB evolution yields the AGB termination luminosity, the core mass of the star at that time, the mass in the nearby circumstellar environment of the remnant star, and the phase of the shell flash cycle at which the star leaves the AGB. Since this star will evolve to become a planetary nucleus (PNN), an outcome of the calculations will be PNN mass, luminosity, and phase of shell flash cycle as a function of initial mass. Combined with the evolutionary tracks of these objects,

[1] Mount Stromlo and Siding Spring Observatories, The Australian National University, Private Bag, Weston Creek P.O., A.C.T. 2611, Australia.
[2] Currently at Space Telescope Science Institute.

such data are capable of providing the PN luminosity function and the input required for computation of the UV flux generated by hot stars passing to the white dwarf phase. These problems will be considered in future papers. We note that extensive studies of PNs in the Magellanic Clouds have been carried out in recent times (Monk, Barlow, & Clegg 1988; Boroson & Liebert 1989; Meatheringham & Dopita 1991a, b; Vassiliadis et al. 1992), and these studies provide a large homogeneous sample of PNs at a single distance with which theoretical calculations can be compared.

A totally separate problem that AGB calculations seek to address is that of S and C star formation. The large body of observational material obtained for late-M and C stars in the Magellanic Clouds (Westerlund et al. 1991 and references therein) provides a strong reference point for comparing theory with observation. However, available stellar evolution models cannot readily explain the formulation of C stars at the low luminosities observed (see Lattanzio 1989a for a review), and the current set of calculations also suffer from this problem.

In this paper we present a grid of 22 stellar evolutionary tracks, complete from the main sequence through to the termination of the AGB. Since the evolution has been followed from the main sequence, it is possible to investigate AGB properties as a function of initial stellar mass and total stellar age. The models span a range in initial mass of $0.89 \lesssim M/M_{\odot} \leq 5.0$. The abundances were chosen to be appropriate for stars in the solar neighborhood, the LMC and the SMC.

2. COMPUTATIONAL DETAILS

The calculations presented in this work were made with the Mount Stromlo Stellar Structure Program (Wood & Zarro 1981; Wood & Faulkner 1986, 1987). Models typically contained 400 mesh points, going up to 500 at shell flashes.

Four values of the metal abundance were used during the calculations: $Z = 0.016$, $Z = 0.008$, $Z = 0.004$ and $Z = 0.001$. The metal abundance $Z = 0.016$ corresponds to the solar mix of Ross & Aller (1976). Metal abundances $Z = 0.008$ and $Z = 0.004$ were adopted to approximate the LMC and SMC abundances, respectively, to agree with the abundance analyses of Russell & Bessell (1989) and Russell & Dopita (1990) which indicate that the present-day LMC metal abundance is $\sim\frac{1}{2}$ solar and the SMC is $\sim\frac{1}{4}$ solar. These abundance analyses also indicate that ^{14}N is less abundant in the LMC and SMC than in the Sun by additional factors of ~ 2 and ~ 4, respectively, and the adopted LMC and SMC mixtures have ^{14}N abundances of 1/4 solar and 1/16 solar, respectively. The $Z = 0.001$ mixture is simply 1/16 solar, and is designed to simulate an old (low mass) population.

All evolutionary sequences were begun with a ^{4}He mass fraction of $Y = 0.25$. This helium abundance is representative of the pregalactic He abundance (Wagoner 1973; Steigman 1983) and of the H II regions in the Magellanic Clouds (Dufour 1984), and gives good fits to color-magnitude diagrams of clusters (e.g., Buzzoni et al. 1983; Caputo, Martinez Roger, & Paez 1987).

Opacities with appropriate values of H, He, C, N, O, and heavier elements (in the Ross-Aller mix ratio) were generated from the Astrophysical Opacity Library of Huebner et al. (1977). A molecular opacity contribution was added to the surface opacity as described in the appendix of Bessell et al. (1989) (however, note that the term 6.56 in the equation for CN + CO opacity should be 1.84 and that the terms 5.97 and 0.005 in the equation for H_2O + TiO opacity should be 1.13 and 0.05, respectively).

Convection was treated by standard mixing-length theory (Cox & Giuli 1968), with mixing-length to pressure scale height ratio $\alpha = 1.6$. No overshoot (e.g., Maeder 1975; Bertelli et al. 1985; Alongi et al. 1991; see also Andersen, Nordström, & Clausen 1990) or extra-mixing (Hollowell & Iben 1988) was used. Semi-convention during He core burning has been treated explicitly using the method of Castellani et al. (1985). Another convective phenomenon that needs to be considered during the core helium-burning exhaustion phase is that of breathing pulses (Castellani, Giannone, & Renzini 1971; Sweigert & Demarque 1972). There is some debate as to whether this phenomenon occurs in real stars. The problem has been addressed by comparing relative numbers of horizontal branch (HB) and AGB stars in globular clusters (Chiosi, Bertelli, & Bressan 1987; Renzini & Fusi Pecci 1988; Caputo et al. 1989). These comparisons suggest that models which suppress breathing pulse appear best able to reproduce the observed ratios of AGB to HB stars. We have therefore suppressed breathing pulses in our calculations by allowing any attempted breathing of the core to mix in just enough helium to maintain the central He mass fraction but not to increase it.

Nuclear reaction rates for hydrogen burning were taken from Harris et al. (1983) when available, and Fowler, Caughlan, & Zimmermann (1975) otherwise. For He burning and beyond, new rates have been adopted from Caughlan & Fowler (1988). The main difference between these new rates and those used previously is that the rate for the reaction $^{12}C(\alpha, \gamma)^{16}O$ has decreased by a factor of ~ 3 from the value published by Caughlan et al. (1985)—the rate is lowered to approximately its 1975 value.

The primary purpose of this work is to study AGB evolution using a realistic prescription of the mass-loss rate. As pointed out in the Introduction, the widely used Reimers (1975) rate does not predict the superwind mass-loss rates required for the production of planetary nebulae (Renzini 1981) or the high mass-loss rates (e.g., Knapp & Morris 1985) observed in AGB stars, and neither does it accurately reflect the increase in mass loss during ascent of the AGB (Wood 1986).

No complete theory of mass loss from AGB stars exists at present, although mass loss is thought to be a dual process involving levitation of matter above the photosphere by large-amplitude radial pulsation followed by the formation of grains on which radiation pressure acts to drive the circumstellar material away from the star (Wood 1979; Castor 1981; Holzer & MacGregor 1985; Bowen 1988; Hearn 1990). The involvement of pulsation in the mass-loss process suggests that the mass-loss rate may be a function of pulsation period. Empirical plots (Wood 1986, 1990a; Schild 1989) of $\log \dot{M}$ against pulsation period P for mass-losing AGB stars show two distinct phases of mass loss. For periods less than ~ 500 days, the mass-loss rate increases exponentially with period, while beyond ~ 500 days, the mass-loss rate is essentially constant at superwind values of a few times $10^{-5}\ M_{\odot}\ \mathrm{yr}^{-1}$. Examination of mass-loss rates for AGB stars in this superwind phase shows that in the Galaxy (Knapp 1986), the LMC (Wood et al. 1992), and the Galactic bulge (Whitelock, Feast, & Catchpole 1991), the mass-loss rate lies within a factor of ~ 2 of the value

$$\dot{M} = L/cv_{\mathrm{exp}}\ , \qquad (1)$$

which corresponds to a radiation-pressure-driven wind. In this equation, L represents stellar luminosity, c represents the speed

of light, and v_{exp} denotes the stellar wind expansion velocity far from the central star. The fact that this relation applies to a mixture of stars in the local Galactic Disk, to young upper AGB stars in the metal-deficient LMC, and to a population that is probably old and metal rich in the Galactic bulge suggests that this relation applies universally (to within a factor of ~ 2). We note that theoretical models of dust-driven winds allow values of $\beta = \dot{M}cv_{exp}/L$ up to ~ 2 (Lèfevre 1989).

A plot of empirically determined mass-loss rates for Mira variables and pulsating OH/IR stars is shown in Figure 1. Mass-loss rates for objects classified as Mira variables and with $P < 1000$ days are observational determinations which have been derived from the CO microwave emission from the stellar wind (Knapp & Morris 1985; Knapp 1985, 1986; Zuckerman, Dyck, & Claussen 1986; Zuckerman & Dyck 1986; Wannier & Sahai 1986; Olofsson, Eriksson, & Gustaffson 1988; Knapp et al. 1989; Margulis et al. 1990; Heske 1990). The mass-loss rates given in these references (or derived from the formulae in Knapp & Morris 1985 in the few cases where no mass-loss rate is given) were adjusted for changes in the adopted stellar distances, which were computed here by assuming the stars lie on the $K - \log P$ relation for Galactic Mira variables (Wood 1990a). K-magnitudes were obtained from Gezari, Schmitz, & Mead (1984). For objects with $P > 1000$ days and very thick dust shells, the CO microwave emission no longer gives a reliable measure of the mass-loss rate (Heske et al. 1990). For these stars, the mass-loss rates shown in Figure 1 were derived from the 60 μm *IRAS* fluxes using the formula of Jura (1987). The Galactic objects were taken from Heske et al. (1990) and the LMC objects from Wood et al. (1992).

As noted above and shown in Figure 1, the mass-loss rate increases exponentially with P before the superwind phase (which starts at $P \sim 500$ days). In this phase, the mass-loss rate used here is that given by equation (8a) of Wood (1990a), viz.,

$$\log \dot{M}(M_\odot \text{ yr}^{-1}) = -11.4 + 0.0123P \text{ (days)} . \quad (2)$$

The mass-loss rate applying at any time during the calculations was assumed to be the minimum of those given by equations (1) and (2). We note that low on the AGB, the mass-loss rate given by equation (2) is much less than the rate given by Reimer's (1975) formula (see Wood 1986).

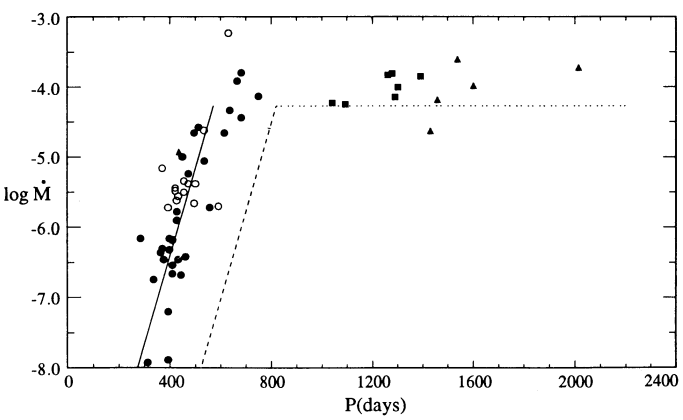

FIG. 1.—Mass-loss rate $\dot{M}(M_\odot \text{ yr}^{-1})$ plotted against period for Galactic Mira variables of spectral type M and S (*filled circles*) and C (*open circles*), and for pulsating OH/IR stars in the Galaxy (*triangles*) and the LMC (*squares*). The solid line is the analytic fit used for low-mass ($M < 2.5\ M_\odot$) stars with the mass-loss rates less than the radiation-pressure-driven limit. The dashed line is the equivalent relation for a 5 $M_\odot$ star, while the dotted line corresponds to mass loss at the radiation-pressure-driven limit for a typical intermediate mass (5 $M_\odot$) LPV in the LMC with $M_{bol} = -6.5$ and $v_{exp} = 12\,\text{km s}^{-1}$.

In order to compute the mass-loss rate from equation (1), v_{exp} needs to be known. This was calculated from equation (9) from Wood (1990a), viz.,

$$v_{exp}(\text{km s}^{-1}) = -13.5 + 0.056P \text{ (days)} , \quad (3)$$

with the additional constraint that v_{exp} lie in the range 3.0–15.0 km s^{-1}. In practice, v_{exp} is almost always 15 km s^{-1} in the superwind phase, in agreement with the expansion velocity observed in high mass-loss rate OH/IR stars (e.g., Eder, Lewis, & Terzian 1988).

Calculation of the mass-loss rate from equation (2) requires a knowledge of the pulsation period P. The computed value of P clearly depends on the mode of pulsation. We adopt the arguments put forward by Willson (1982) and Wood (1990a, b) and assume that Mira variables and dust-enshrouded variable AGB stars are pulsating in the fundamental mode (see Tuchman 1991 for alternative arguments). Then P can be derived using the period-mass-radius relation given by equation (5) of Wood (1990a):

$$\log P \text{ (days)} = -2.07 + 1.94 \log R/R_\odot - 0.9 \log M/M_\odot . \quad (4)$$

The above equations predict that stars of low mass ($\lesssim 2.5\ M_\odot$) will attain superwind-like mass-loss rates at $P \sim 500$ days when they will become dust enshrouded and no longer optically visible. This is what is observed in low-mass populations such as those in the solar vicinity, where the number density of optically visible Mira variables drops sharply between $P = 425$ and 500 days (Wood & Cahn 1977). Similarly, in the Galactic Bulge, the long period variable (LPV) population is optically visible up to $P = 500$ days (Lloyd Evans 1976; Wood & Bessell 1983) while at longer periods it can only be seen in the infrared (Whitelock et al. 1991).

On the upper AGB where masses are $\sim 5\ M_\odot$ and $M_{bol} \sim -6$ to -7, optically visible LPVs exist out to periods of ~ 750 days (Wood, Bessell, & Fox 1983; Hughes & Wood 1990). In order to prevent the adopted mass-loss prescription removing these observed objects, equation (2) was modified to delay the onset of the superwind phase in stars of mass greater than 2.5 $M_\odot$. For these stars, the mass-loss rate was derived from the equation

$$\log \dot{M}(M_\odot \text{ yr}^{-1}) = -11.4 + 0.0125[P(\text{days}) - 100(M/M_\odot - 2.5)] . \quad (5)$$

The dependence of mass loss on period for a typical 5 $M_\odot$ star is shown in Figure 1.

In summary, the above AGB mass-loss scheme reproduces the observed rapid exponential increase in mass-loss rate with period before the onset of the superwind phase, it has a superwind phase corresponding to radiation-pressure-driven mass loss, and it predicts the onset of this superwind mass-loss phase at pulsation period where optically visible LPVs disappear in the solar vicinity, the Galactic Bulge, and the LMC.

For the purposes of this paper, the AGB mass-loss phase is assumed to be complete when the envelope mass is reduced to such a small value that log T_{eff} has become hotter than a reference AGB temperature by an amount $\Delta \log T_{eff} = 0.3$,

where the reference AGB is given by

$$M_{\rm bol} = 12.5 \log T_{\rm eff} - 2.925 \log M/M_{\odot} + 1.453 \log Z/Z_{\odot} - 47.1 . \quad (6)$$

This reference AGB temperature is a fit to the AGB temperatures produced by the evolution code for stars with evolution masses sufficiently large that the star has not begun to evolve to the blue. Some preliminary sequences were run in order to derive the fit. The period of pulsation used in the mass-loss equations (2) and (5) was derived assuming the star had a $T_{\rm eff}$ given by equation (6) (rather than the actual $T_{\rm eff}$). This was done so that the superwind mass-loss rate would be maintained while the star evolved to the blue of the AGB, where the superwind ceased at $\Delta \log T_{\rm eff} = 0.3$.

AGB mass loss accounts for the majority of the mass lost in most low- to intermediate-mass stars. However, in low-mass globular cluster stars, mass loss amounting to $\sim 0.2\ M_{\odot}$ is required on the first giant branch (FGB) in order to match the observed HB morphology (Fusi Pecci & Renzini 1976, 1978; Renzini & Fusi Pecci 1988, and references therein). (But we note here that recent results of Simon 1992 indicate that the well-established first giant branch mass loss of $\sim 0.2\ M_{\odot}$ may be negligible after all!) If we adopt the Reimers (1975) mass-loss rate on the FGB, then the mass-loss rate is proportional to R/M, and the amount of envelope mass lost on the FGB increases as M is reduced (apart from the direct effect of M on the Reimers mass-loss rate, lowering M also gives a cooler giant branch which increases R and further increases $\dot{M}$). In these calculations, we have only considered FGB mass loss for evolutionary sequences with initial mass $M_i < 1\ M_{\odot}$ where the mass lost is a significant fraction of the envelope mass on the early AGB. The mass-loss rate used was actually one third the Reimers (1975) rate in order to get a total mass loss of $\sim 0.2\ M_{\odot}$ on the FGB for the lowest mass evolved stars. A detailed calculation showing the dependence of total FGB mass loss under the assumption of a Reimers mass loss law is shown in Figure 8 of Sweigert, Greggio, & Renzini (1990) (although these authors used a mass-loss rate that was two thirds Reimers').

3. RESULTS AND DISCUSSION

All evolutionary sequences in this study were begun on the zero-age main sequence and went through to the end of the AGB. Although the study of AGB evolution with realistic mass-loss rates is the prime motivation for these calculations, we briefly look at some properties of the stellar models prior to the thermally pulsing AGB.

3.1. *Evolution to the Thermally Pulsing AGB*

In Table 1 we have summarized the evolutionary lifetimes of various phases, including the AGB phase. The main-sequence (MS) lifetime, $\tau_{\rm MS}$, has been defined as the time the central hydrogen abundance drops to zero. The interval $\tau_{\rm FGB}$ is calculated from the end of the MS to the point of He core ignition and includes the time spent on the sub-giant or H-shell narrowing phase, which varies from 40%–60% of $\tau_{\rm FGB}$. The definition of $\tau_{\rm FGB\text{-}C}$ depends on the stellar mass: for stars with $M \leq 2.0\ M_{\odot}$ which develop degenerate cores on the FGB, it is the time taken to evolve up the FGB from the luminosity of the helium core burning clump to the point of He core ignition; for more massive stars it is the lifetime from the minimum luminosity of the FGB up to the point of helium ignition. The He core burning lifetime $\tau_{\rm HeB}$ is defined as the time from core helium ignition to the time of central He core exhaustion which is well defined by a peak in the H-shell luminosity. The early AGB lifetime $\tau_{\rm EAGB}$ is defined as the time from central helium exhaustion to the time of the first major helium shell flash, while the thermally pulsing AGB lifetime $\tau_{\rm TPAGB}$ is defined as the remainder of the lifetime (until the star moves away from the AGB by an amount $\Delta \log T_{\rm eff} = 0.3$). The total AGB life-

TABLE 1

LIFETIMES OF MAJOR EVOLUTIONARY PHASES

M ($M_{\odot}$)	Z	$\tau_{\rm MS}$ (yr)	$\tau_{\rm FGB\text{-}C}$ (yr)	$\tau_{\rm FGB}$ (yr)	$\tau_{\rm HeB}$ (yr)	$\tau_{\rm EAGB}$ (yr)	$\tau_{\rm TPAGB}$ (yr)	$\tau_{\rm AGB}$ (yr)	$\frac{\tau_{\rm FGB\text{-}C}}{\tau_{\rm HeB}}$	$\frac{\tau_{\rm AGB}}{\tau_{\rm FGB\text{-}C}}$	$\frac{\tau_{\rm TPAGB}}{\tau_{\rm EAGB}}$	$\frac{\tau_{\rm AGB}}{\tau_{\rm HeB}}$
1.0	0.016	1.125E+10	5.786E+07	3.563E+09	1.416E+08	1.209E+07	4.946E+05	1.258E+07	0.409	0.218	0.041	0.089
1.5	0.016	2.742E+09	5.197E+07	7.570E+08	1.359E+08	9.191E+06	8.266E+05	1.002E+07	0.373	0.193	0.090	0.038
2.0	0.016	1.236E+09	5.454E+07	1.648E+08	1.509E+08	7.933E+06	1.175E+06	9.108E+06	0.361	0.167	0.148	0.060
2.5	0.016	6.192E+08	1.429E+08	4.283E+07	2.805E+08	1.084E+07	2.184E+06	1.303E+07	0.051	0.911	0.201	0.046
3.5	0.016	2.307E+08	1.669E+06	1.110E+07	9.142E+07	2.793E+06	4.270E+05	3.220E+06	0.018	1.929	0.153	0.035
5.0	0.016	9.560E+07	3.638E+05	2.578E+06	2.353E+07	1.145E+06	2.624E+05	1.408E+06	0.015	3.869	0.229	0.060
0.945	0.008	1.052E+10	6.094E+07	3.038E+09	1.356E+08	1.057E+07	5.704E+05	1.114E+07	0.449	0.183	0.054	0.082
1.0	0.008	8.129E+09	4.860E+07	2.776E+09	1.336E+08	9.600E+06	6.502E+05	1.025E+07	0.364	0.211	0.068	0.077
1.5	0.008	2.461E+09	3.450E+07	5.140E+08	1.304E+08	7.783E+06	9.385E+06	8.721E+06	0.265	0.253	0.121	0.067
2.0	0.008	1.018E+09	4.458E+07	1.286E+08	1.520E+08	1.340E+07	1.339E+06	1.474E+07	0.293	0.331	0.100	0.097
2.5	0.008	5.170E+08	9.028E+06	3.355E+07	2.209E+08	1.035E+07	1.827E+06	1.217E+07	0.041	1.349	0.177	0.055
3.5	0.008	2.009E+08	1.100E+06	9.042E+06	6.388E+07	3.032E+06	3.509E+05	3.383E+06	0.017	3.075	0.116	0.053
5.0	0.008	8.567E+07	2.496E+05	2.426E+06	2.161E+07	8.036E+05	3.601E+05	1.150E+06	0.012	4.662	0.448	0.053
0.89	0.004	1.096E+10	6.276E+07	2.617E+09	1.294E+08	1.127E+07	7.711E+05	1.204E+07	0.485	0.192	0.068	0.093
1.0	0.004	6.650E+09	5.872E+07	2.111E+09	1.279E+08	8.008E+06	8.684E+05	8.875E+06	0.459	0.151	0.108	0.069
1.5	0.004	2.088E+09	3.650E+07	4.202E+08	1.268E+08	6.302E+06	9.667E+05	7.269E+06	0.288	0.199	0.153	0.057
2.0	0.004	8.930E+08	3.693E+07	1.082E+08	1.539E+08	6.705E+06	1.559E+06	8.264E+06	0.240	0.224	0.233	0.054
2.5	0.004	4.604E+08	5.953E+06	2.745E+07	1.669E+08	5.149E+06	1.248E+06	6.397E+06	0.036	1.075	0.242	0.038
3.5	0.004	1.844E+08	7.070E+05	6.868E+06	5.355E+07	2.150E+06	2.524E+05	2.402E+06	0.013	3.398	0.117	0.045
5.0	0.004	8.058E+07	1.759E+05	2.180E+06	1.864E+07	5.924E+05	3.123E+05	9.205E+05	0.009	5.143	0.527	0.049
1.0	0.001	5.737E+09	3.436E+07	1.344E+09	1.211E+08	7.737E+06	1.357E+06	9.094E+06	0.284	0.265	0.175	0.075
1.5	0.001	1.603E+09	3.633E+07	3.606E+08	1.222E+08	4.962E+06	1.127E+06	6.088E+06	0.297	0.168	0.227	0.050

time τ_{AGB} is the sum of τ_{EAGB} and τ_{TPAGB}. Table 1 also lists ratios of various lifetimes, these ratios being equivalent to population ratios in the various evolutionary phases. Figure 2 shows a representative set of evolutionary tracks for the LMC composition $(Y, Z) = (0.25, 0.008)$.

Comparison of MS lifetimes from the present study with those of Lattanzio (1991) and Castellani, Chieffi, & Straniero (1992) shows good agreement, generally to 3% for the lower masses and to ~10% for higher masses. However, the ages given by the Sweigert, Greggio, & Renzini (1989) models are ~30% smaller than those presented here. The difference can probably be attributed to the use by Sweigert et al. (1989) of the older Cox & Stewart (1970a, b) opacities rather than the Huebner et al. (1977) opacities. This discrepancy has been noted previously, and it is found to become more severe with increasing Z (VandenBerg & Laskarides 1987).

An important point to note about the present calculations is that the last 5%–10% of core helium burning (CHeB) is included in the calculations along with an explicit treatment of semi-convection (as opposed to letting ordinary convection mix the core as in Lattanzio's calculations). Many calculations in the past have tended to ignore the final CHeB phase due to the uncertainty associated with the treatment of breathing pulses (e.g., Sweigert 1987). Calculation through the final phases of core He burning increases the total CHeB lifetime. It also increases the final O/C abundance ratio in the core as this ratio increase markedly toward the end of CHeB (Sweigert & Gross 1976). A comparison of our clump burning lifetimes with those of Lattanzio (1991) (who also evolved right through the helium core burning stage) shows close agreement, whereas the lifetimes of Seidel, Demarque, & Weinberg (1987) (who stopped their calculations when the central helium abundance reached $X_{He} \sim 0.1$) are ~30% shorter. In another comparison, values of τ_{HeB} from Castellani et al. (1992) (who evolved completely through the He core burning phase) are ~15% shorter than the corresponding values in this study.

The central ^{12}C and ^{16}O abundances following core He burning for our $M_i \leq 2.5\ M_\odot$ models are $X_C \sim 0.1$ and $X_O \sim 0.9$, respectively. This is despite the fact that we are using the new, reduced $^{12}C(\alpha, \gamma)^{16}O$ reaction rate. The models presented by Lattanzio (1991), who used the $^{12}C(\alpha, \gamma)^{16}O$ reaction rate which is similar to the one used here, have $X_C \sim 0.2$–0.3 and $X_O \sim 0.7$–0.8. Nearly all the conversion of ^{12}C to ^{16}O occurs during the burning of the last 10% of He in the core. Our high rates of conversion are almost certainly the result of our treatment of semiconvection/breathing pulses which appears to be more efficient at mixing helium into the core and prolonging the last stages of CHeB than most codes. Models with $M_i \geq 3.5\ M_\odot$ have cores with $X_C \sim 0.45$ and $X_O \sim 0.55$, similar to the abundance in Lattanzio's (1991) $5\ M_\odot$ models.

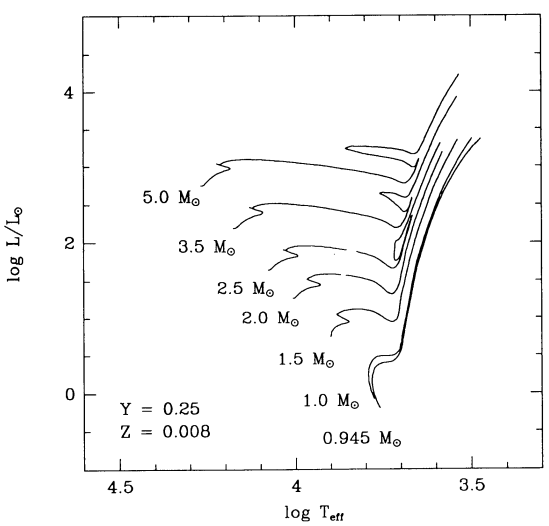

FIG. 2.—H-R diagram for evolutionary sequences calculated in this study with $(Y, Z) = (0.25, 0.008)$. For $M_i \geq 2.5\ M_\odot$, the tracks end at the first helium shell flash, while for $M_i < 2.5\ M_\odot$ the tracks end at the helium core flash.

The duration of the early-AGB (E-AGB) phase (the interval from He core exhaustion to the onset of the first major helium shell flash) in theoretical calculations depends very strongly on the treatment of the preceding CHeB evolution. In particular, the relative time scales of the CHeB and E-AGB phases depend on the amount of mixing of He into the core through semiconvection, core overshoot, and breathing pulses. Mixing in more He during core helium burning extends the CHeB phase at the expense of the E-AGB phase. The ratio of AGB to CHeB lifetimes in our lowest mass models is $\tau_{AGB}/\tau_{HeB} \sim 0.08$, which is similar to the value Caputo et al. (1989) obtained when they included breathing pulses in their models. This result gives added weight to the suggestion above that our treatment of central helium exhaustion extends this phase longer than most codes which suppress breathing pulses.

Finally, we note that up to the end of the E-AGB phase, with our mass-loss formalism, the total stellar mass remains essentially unchanged from its main-sequence mass (or the mass at the end of the FGB for the two sequences where FGB mass loss was included).

3.2. *AGB Evolution with Mass Loss: The Thermally Pulsing AGB Phase*

The variation with time of luminosity, effective temperature, wind expansion velocity, total mass, mass-loss rate, and pulsation period during the thermally pulsing AGB (TP-AGB) phase is depicted in Figures 3–9 for the seven evolutionary sequences studied here with abundance $(Y, Z) = (0.25, 0.008)$ and mass 0.945–5.0 $M_\odot$. The behavior shown in these plots is typical of the behavior of stars at other abundances. The dotted line to the right of each diagram represents the end of the AGB phase, defined here to be the point where the star has evolved away from the AGB until the effective temperature is 0.3 dex larger than the effective temperature given by equation (6). We now examine various aspects of the behavior of models during the TP-AGB phase.

3.2.1. *The Superwind Mass-Loss Phase*

A striking feature of the mass-loss behavior shown in Figures 3–9 is the sudden onset of superwind phases with $\dot{M} = L/cv_{exp}$, the radiation pressure limit. For $M_i \lesssim 2.5\ M_\odot$, the mass-loss rate reaches the radiation pressure limit only during the last 2–3 thermal pulse cycles, and between the superwind phases are periods of diminished mass loss coinciding with the extended luminosity dips characteristic of thermal pulses experienced by low-mass stars. For larger masses, mass loss is maintained at the radiation-pressure-driven limit over many cycles, with less significant variation in mass-loss rate as thermal pulses occur.

The rapidity with which the mass-loss rate builds up to superwind values at first seems surprising. Several factors contribute. Firstly, the mass-loss rate increases exponentially

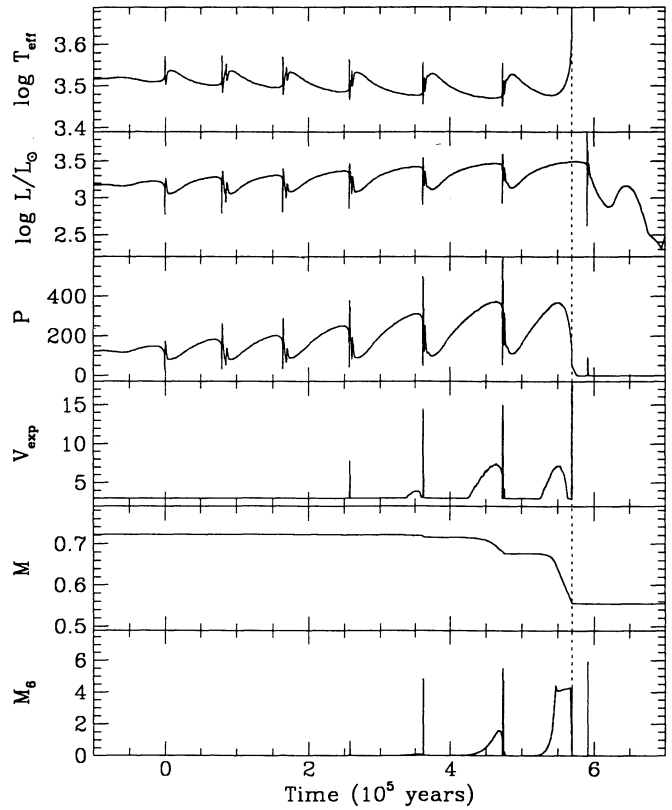

FIG. 3.—Time dependence of various quantities during the TP-AGB phase of a star with $(M, Y, Z) = (0.945, 0.25, 0.008)$. The abscissa represents the time after the first major thermal pulse. The dotted vertical line at right represents the end of the AGB phase, as defined in the text. M_6 is the mass-loss rate in units of $10^{-6}\ M_\odot\ \mathrm{yr}^{-1}$.

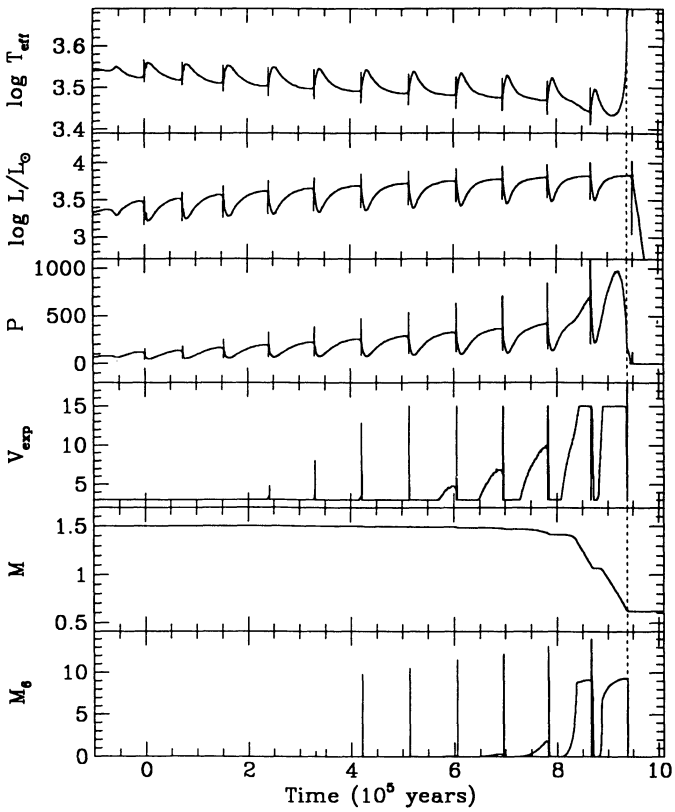

FIG. 5.—Same as Fig. 3, except for $(M, Y, Z) = (1.5, 0.25, 0.008)$

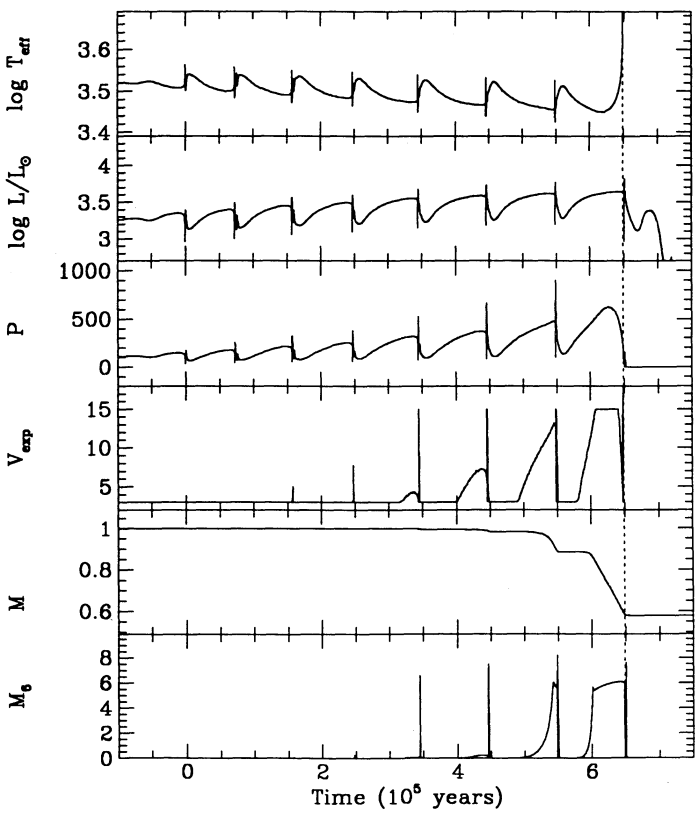

FIG. 4.—Same as Fig. 3, except for $(M, Y, Z) = (1.0, 0.25, 0.008)$

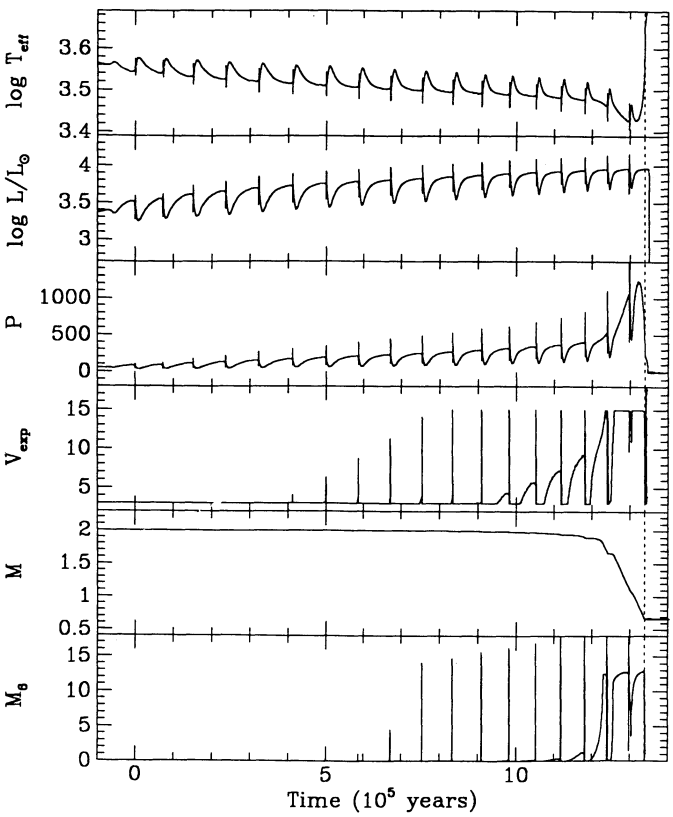

FIG. 6.—Same as Fig. 3, except for $(M, Y, Z) = (2.0, 0.25, 0.008)$

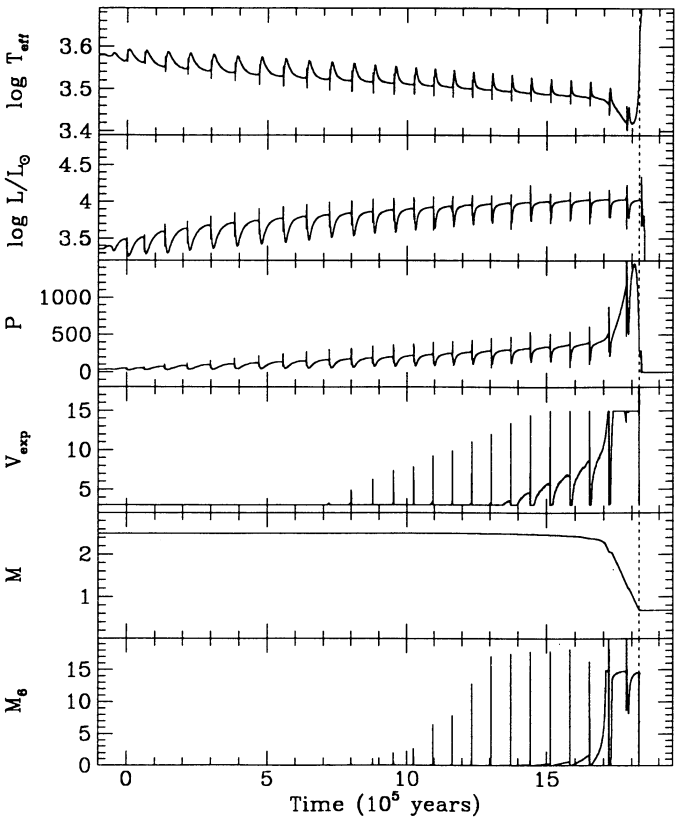

FIG. 7.—Same as Fig. 3, except for $(M, Y, Z) = (2.5, 0.25, 0.008)$

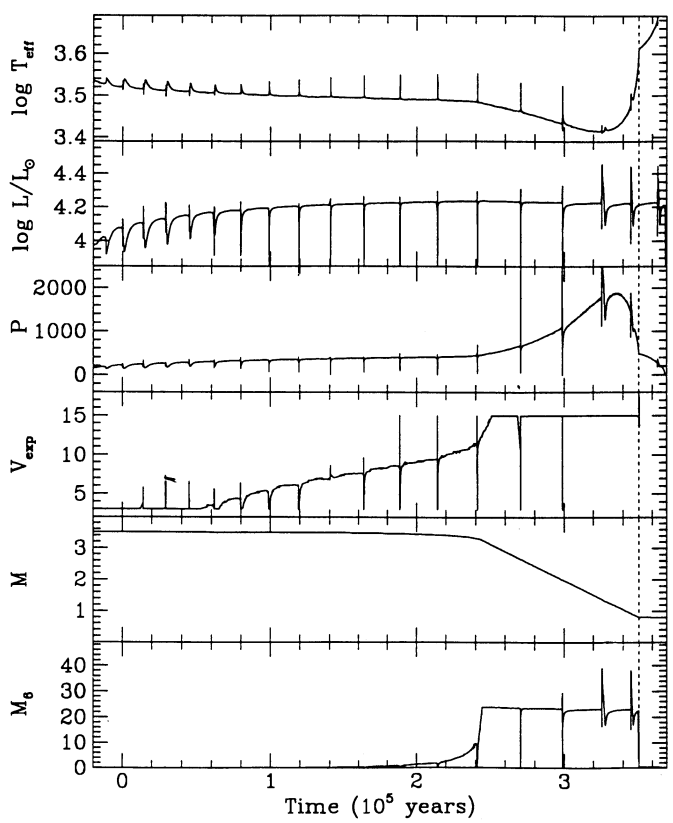

FIG. 8.—Same as Fig. 3, except for $(M, Y, Z) = (3.5, 0.25, 0.008)$

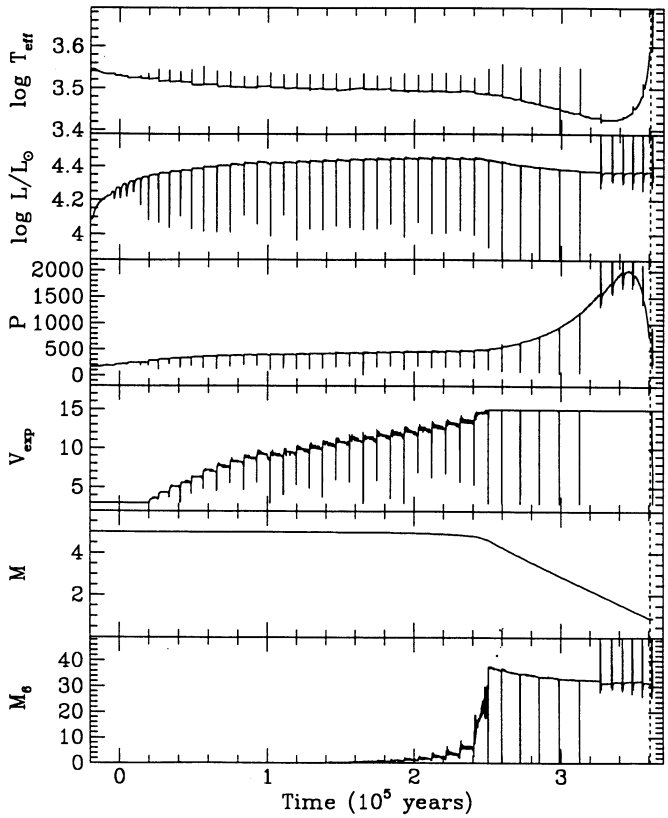

FIG. 9.—Same as Fig. 3, except for $(M, Y, Z) = (5.0, 0.25, 0.008)$

with the pulsation period P, and $P \propto R^{1.94}/M^{0.9} \propto L^{0.97}/M^{0.9}T_{\rm eff}^{3.88}$. As hydrogen burning is reestablished following a thermal pulse, the surface luminosity increases and $T_{\rm eff}$ decreases (see Figs. 3–9), and both factors contribute to increasing P. Then, once significant mass-loss rates develop, M is decreased, leading to a further direct increase in P via its $M^{-0.9}$ dependence, and an indirect increase via the decrease in $T_{\rm eff}$ caused by the movement of the star to a cooler AGB (see eq. [6]). We note that nearly all mass is lost during the quiescent phases, rather than during the luminosity spike at the thermal pulses, because of the short duration of such events. Since the quiescent luminosity is highest immediately prior to each shell flash, superwinds occur preferentially at this time.

The discrete superwind phases noted above suggest that we might expect to see 2–3 circumstellar shells around TP-AGB stars with $M_i \lesssim 2.5\ M_\odot$, provided the older shells have not dispersed into the interstellar medium in the $\sim 10^5$ yr between shell flashes. Indeed, there are now many AGB stars which are known to have hollow shells that are presumably the result of the abrupt cessation of mass loss as a result of a thermal pulse (Willems & de Jong 1986; Chan & Kwok 1988; Zijlstra et al. 1992; Olofsson et al. 1992). Furthermore, if the majority of AGB objects are assumed to evolve into a PN, then the observed mass-loss behavior offers a natural explanation for the detached multiple shell PNs seen in the Galaxy (Kaler 1974; Chu, Jacoby, & Arendt 1987; Frank, Balick, & van der Veen 1992). We note that the mass-loss rates we used for the superwind phase are uncertain by factors of ~ 2. If we had used a superwind rate a factor of 2 higher, the lower mass stars could have ejected all their envelopes in one flash cycle, and multiple shell objects would only be produced by the more

massive stars, or by the lower mass stars when the first superwind phase commenced close to the onset of a thermal pulse.

In Figure 10 we compare various mass-loss processes and formulae during the TP-AGB evolution for the $(M, Y, Z) = (1.5, 0.25, 0.008)$ evolutionary sequence. As well as the adopted mass-loss rate, we show the Reimers rate, the rate of consumption of the envelope by H shell burning, and the radiation-pressure-driven limit mass-loss rate.

For the case depicted in Figure 10, the superwind mass-loss rate (radiation pressure limit) is reached only during the last two thermal pulses, for an average of $\sim 5 \times 10^4$ yr per pulse. The adopted mass-loss rate exceeds the Reimers rate only over the last four thermal pulse cycles. This is an important point since, if the Reimers mass-loss rate is artificially enhanced in order to terminate the AGB at observed luminosities, the mass of an AGB star diminishes gradually up the AGB rather than just at the end as in the present calculations. Since the likelihood of dredge-up of carbon on the AGB is enhanced by a larger envelope mass (Wood 1981), the Reimers mass-loss law may artificially reduce the amount of dredge-up found in theoretical calculations.

3.2.2. *Surface Luminosity Variations*

For low-mass stars, the time dependence of the surface luminosity shown in Figures 3–9 is similar to that found in other studies. Following each thermal pulse, there is a brief (~ 500 yr) pulse of surface luminosity followed by a substantial luminosity dip which lasts for $\sim 20\%$–30% of the flash cycle (e.g., Härm & Schwarzschild 1975; Wood & Zarro 1981; Boothroyd & Sackmann 1988a). The luminosity then rises again to a value which increases slowly with time until the next thermal pulse, when the cycle repeats.

The behavior just described is not exhibited by the higher mass ($M_i \geq 3.5\ M_\odot$) models (see also Iben 1975). In these models the surface luminosity is barely affected by the internal helium shell flashes, at least while the envelope mass remains large ($\gtrsim 1.5\ M_\odot$). However, when the envelope mass has been reduced below $\sim 1.5\ M_\odot$, the type of behavior shown by the low-mass stars begins, with substantial pulses of luminosity reaching the surface at each flash, and prolonged luminosity dips following each flash. This behavior is shown in detail in the top panel of Figure 11 for the $(M, Y, Z) = (5.0, 0.25, 0.016)$ sequence.

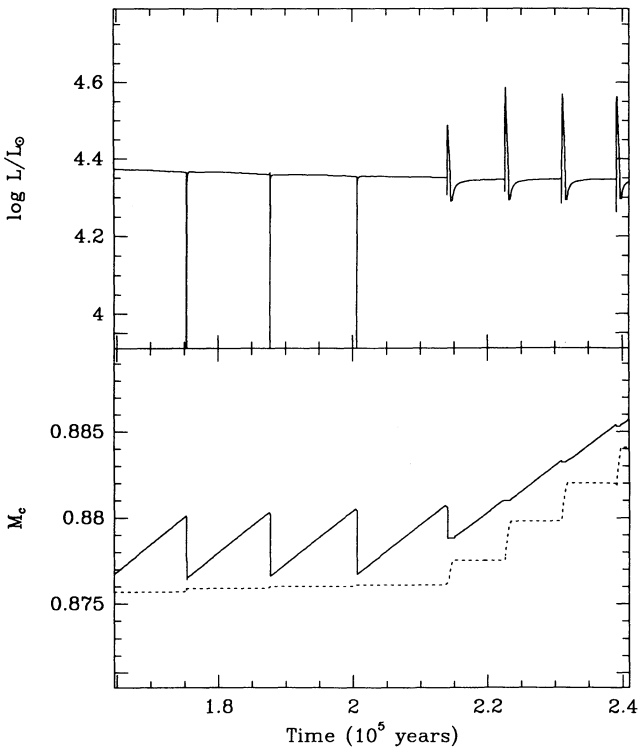

FIG. 11.—The time dependence of surface luminosity (*top panel*) and core mass (*lower panel*) for the $(M, Y, Z) = (5.0, 0.25, 0.016)$ evolutionary sequence. In the lower panel, the solid line represents the hydrogen core mass, and the dotted line represents the helium core mass. The change in flash cycle characteristics with time is due to the decrease in envelope mass. The abscissa represents the time since the first thermal pulse, and the first pulse shown is the 22d.

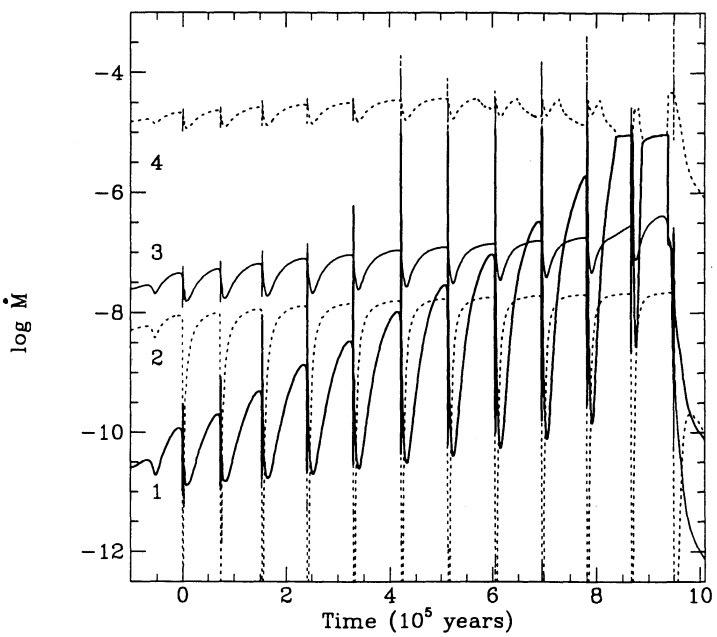

FIG. 10.—Mass-loss behavior for the $(M, Y, Z) = (1.5, 0.25, 0.008)$ evolutionary sequence. Curve 1 depicts the mass-loss rate applied in the stellar evolution calculation; curve 2 represents mass lost via H burning; curve 3 represents the canonical Reimers mass-loss rate with $\eta = \frac{1}{3}$; and curve 4 represents the radiation-pressure-driven limit mass-loss rate.

The bottom panel of Figure 11 shows why massive stars do not show significant surface luminosity variations. While the envelope is massive, any increase in surface luminosity due to a shell flash causes envelope convection to eat inwards, giving rise to the sawtooth variation in core mass M_c (the base of the convective envelope is essentially coincident with the line representing the hydrogen-exhausted core in Fig. 11). More importantly, the inward advance of the envelope convection cools the He burning shell which is extinguished before it can burn a significant mass of helium. Thus there is only a small amount of energy produced during the shell flash, and the surface luminosity barely changes. The material dredged up at each flash is primarily the helium and nitrogen produced by CNO-cycle hydrogen burning during the previous interflash evolution.

3.2.3. *Luminosity-Core Mass Relations*

Paczyński (1970) first showed that there was a linear relation between luminosity and core mass for AGB stars, and this has been confirmed by various calculations since then (Iben 1977;

Wood & Zarro 1981; Lattanzio 1986; Boothroyd & Sackmann 1988b). As shown by Boothroyd & Sackmann (1988b), a proper comparison of the available luminosity-core mass (L-M_c) relations in the literature is not a trivial matter, although there is general agreement between the relations derived by different authors. At least that was the situation until Blöcker & Schönberner (1991) noted that the L-M_c relation may not hold for stars with $M_i \geq 7\ M_\odot$ (see also Boothroyd & Sackmann 1992). Blöcker & Schönberner (1991) found that their 7 $M_\odot$ star evolved to a luminosity well above (about 3 times) that expected from standard luminosity-core mass relations for low-mass stars, and they attributed this result to the fact that their 7 $M_\odot$ star had deep envelope convection, the base of which penetrated the hydrogen burning shell. Our 5 $M_\odot$ models have core masses similar to those of Blöcker & Schönberner (1991) and deep envelope convection but they are only slightly more luminous ($\sim$15%) than the canonical L-M_c relation. This is shown for the solar composition models in Figure 12. There is no doubt that massive envelopes and deep envelope convection cause an increase in luminosity for a given core mass since the 5 $M_\odot$ sequences all show a clear *decrease* in luminosity with time as the envelope mass is reduced by mass loss from $\sim$4 $M_\odot$ to $\sim$1.5 $M_\odot$. At this point, a radiative layer separates the hydrogen burning shell from the envelope convection, and the core burning luminosity becomes independent of the envelope parameters (Wood & Zarro 1981) and fits the linear relation characteristic of AGB stars with low envelope mass (Fig. 12).

3.2.4. *Interpulse Time Scales and TP-AGB Lifetimes*

For the evolutionary sequences presented in this study, Figures 13–18 show the variation with time of the interval between the thermal pulses (τ_{TP}), the change in total mass being thermal pulses (m_{TP}), and the recovery time (τ_R) defined as the time from the beginning of a He shell flash to the time when the H shell luminosity recovers to be equal to the He shell luminosity.

Figurs 13–18 show once again that all the mass is lost during the last few thermal pulse cycles. The mass lost per cycle is

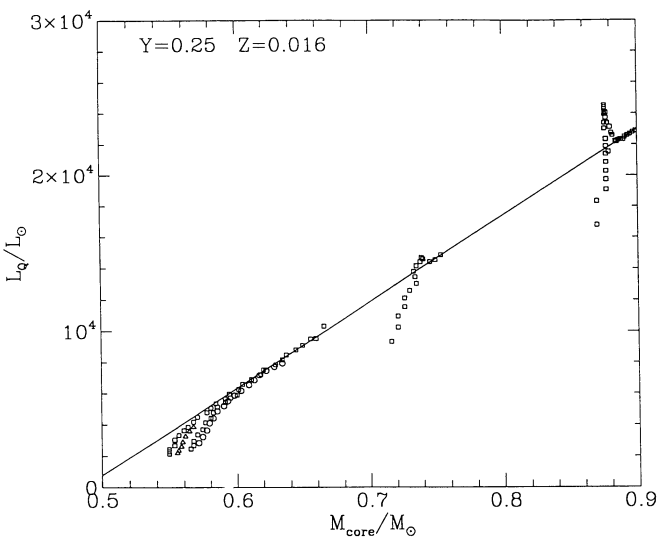

FIG. 12.—Maximum luminosity during quiescent hydrogen burning in thermally pulsing AGB stars of initial masses 1.0, 1.5, 2.0, 2.5, 3.5, and 5.0 $M_\odot$. The line is a fit to the luminosity-core mass relation for stars of low envelope mass.

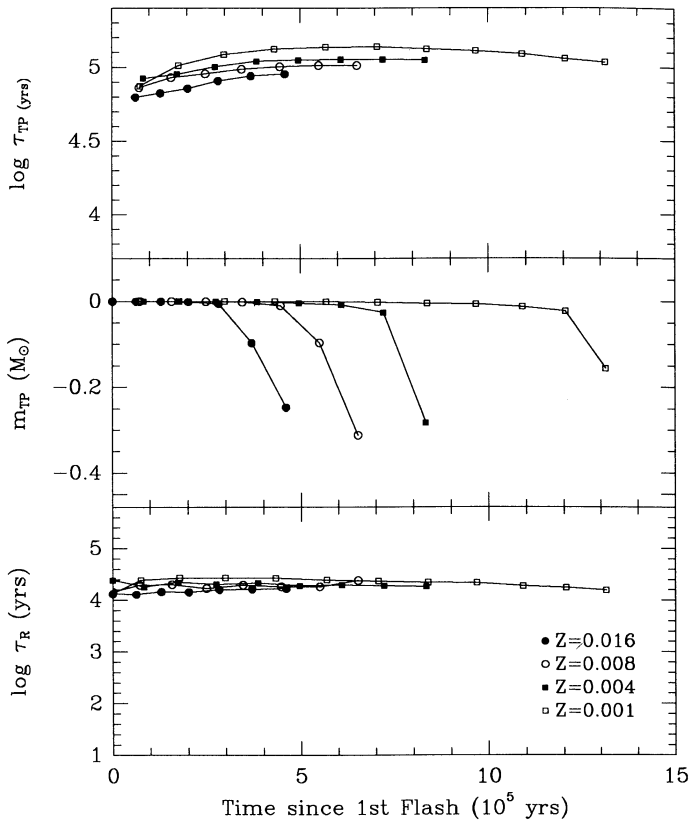

FIG. 13.—The variation in inter-pulse duration τ_{TP} (yr), the change in total stellar mass per cycle m_{TP} ($M_\odot$), and He shell flash recovery time τ_R (yr), for the 1.0 $M_\odot$ evolutionary sequences.

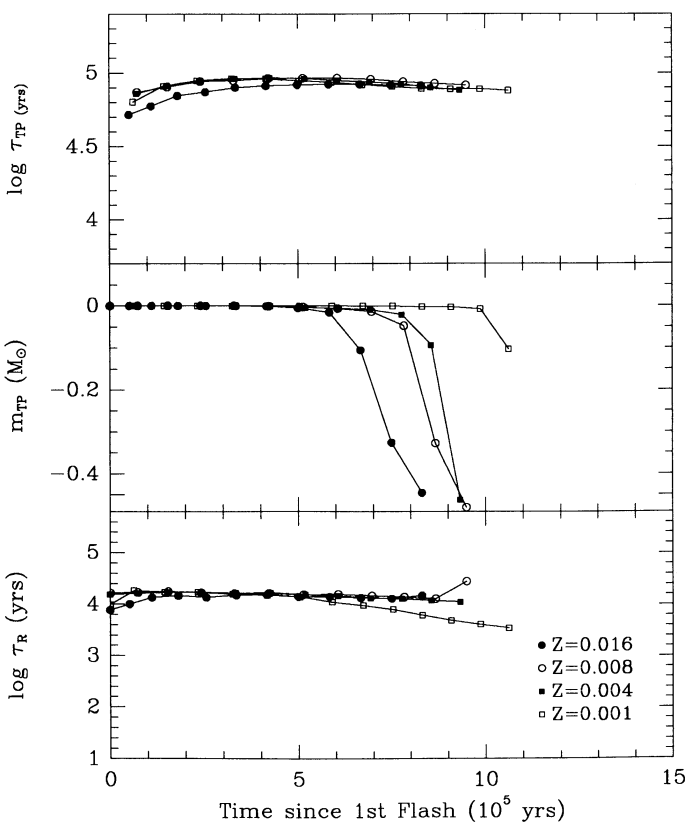

FIG. 14.—Same as Fig. 13, except for 1.5 $M_\odot$ evolutionary sequences

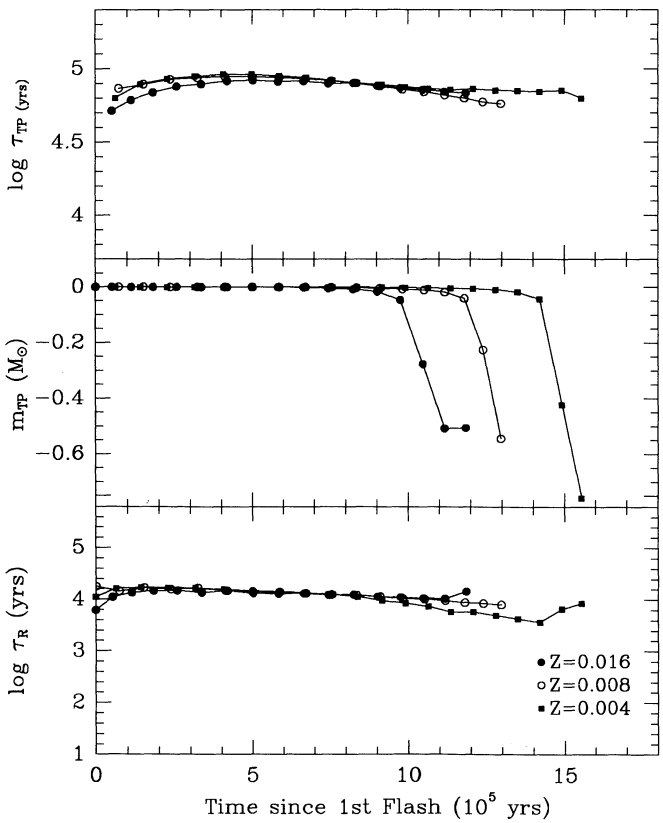

FIG. 15.—Same as Fig. 13, except for 2.0 $M_\odot$ evolutionary sequences

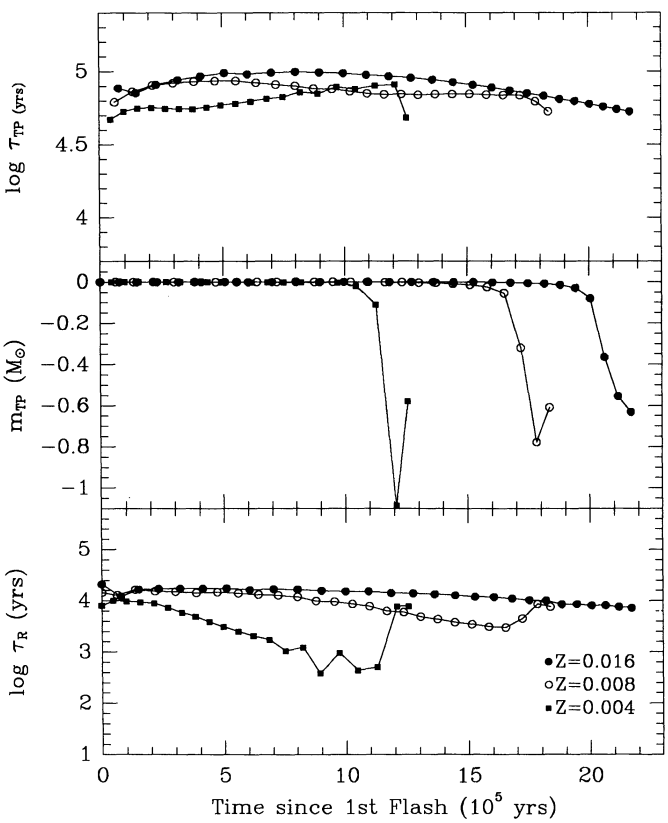

FIG. 16.—Same as Fig. 13, except for 2.5 $M_\odot$ evolutionary sequences

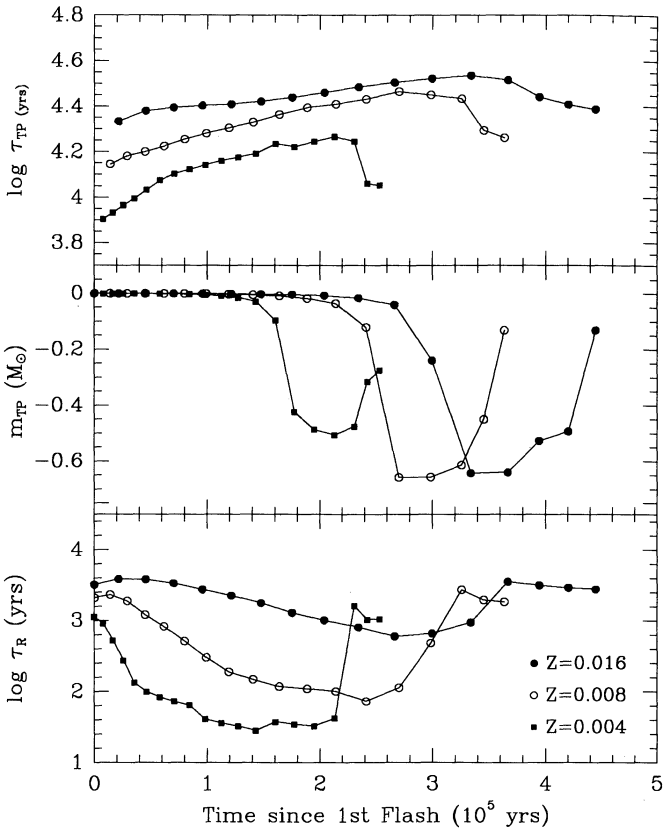

FIG. 17.—Same as Fig. 13, except for 3.5 $M_\odot$ evolutionary sequences

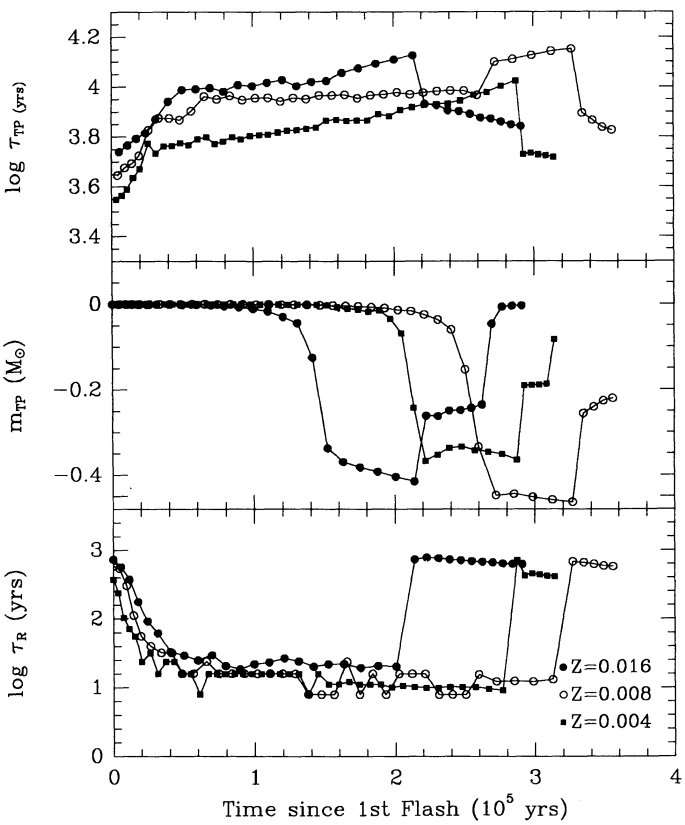

FIG. 18.—Same as Fig. 13, except for 5.0 $M_\odot$ evolutionary sequences

$\sim 0.2\ M_\odot$ for stars with $M_i \sim M_\odot$, this mass being the mass of a typical planetary nebula. The maximum mass lost per thermal pulse cycle generally increases with stellar mass but seems to reach a maximum value of $\sim 0.6\ M_\odot$, at least for the solar metallicity models. This limit is a result of the fact that, although the luminosity and mass-loss rate increases with M_i, the decrease in interpulse duration has a counterbalancing effect.

The lower mass ($M_i \lesssim 2\ M_\odot$) sequences show the well-known initial increase in τ_{TP} as the flashes approach full amplitude, followed by the steady decline resulting from the increase in core mass. Comparing the τ_{TP}-M_c relation for $Z = 0.001$ from Boothroyd & Sackmann (1988c) with our $(M, Z) = (1.5, 0.001)$ sequence, we note that our models have slightly larger values of M_c ($\sim 0.01\ M_\odot$) for a given value of τ_{TP}.

The more massive models show a completely different behavior, with τ_{TP} increasing continuously until the onset of heavy mass loss. But mass loss itself does not affect τ_{TP}—it is the disappearance of deep envelope convection that causes τ_{TP} to decrease (see the 3.5 and 5 $M_\odot$ series). Note the large increase in τ_R at this time also, a result of the change in the nature of the surface luminosity variations detailed above. The decrease in the inter-pulse duration caused by lowering of the envelope mass clearly causes a significant decrease in the amount of mass lost per cycle during the superwind phase.

The total TP-AGB lifetime (readily seen in Figs. 13–18 or Table 1) is largely determined by the point of onset of the superwind phase, and it changes in a rather complicated way with both M and Z. For the lower mass ($M_i \lesssim M_\odot$) stars, the AGB lifetime increases with decreasing metallicity due to the fact that low-metallicity stars have warmer giant branches and need to evolve to higher luminosities in order to reach the superwind phase (which starts when $P \sim 500$ days). At 2.5 and 3.5 $M_\odot$, the metallicity dependence is reversed, with high-metallicity sequences lasting the longest. This is due to the higher starting luminosity for lower metallicity sequences at these masses. At 5 $M_\odot$, the TP-AGB lifetime has a maximum value at intermediate ($Z = 0.008$) metallicities.

All metallicities show the same basic variation of total TP-AGB lifetime with mass (Table 1). The lifetime increases from ~ 5 to $\sim 20 \times 10^5$ yr as M increases from 1.0 to 2.5 $M_\odot$ but for heavier masses (3.5 and 5 $M_\odot$) the TP-AGB lifetime drops dramatically to $\sim 3 \times 10^5$ yr. This drop-off in AGB lifetimes for the mass range $2.5 \lesssim M_i \lesssim 5.0$ might offer an explanation for the apparent paucity of objects observed in the LMC on the upper AGB (e.g., Reid & Mould 1985, 1991; Wood, Bessell, & Paltoglou 1985).

A feature of particular interest regarding AGB stars with deep envelope convection is their rate of evolution up the AGB. It has long been known (e.g., Wood 1974) that the linear relation between AGB core mass and luminosity for low-mass AGB stars implies a mean rate of evolution up the AGB of ~ 1 mag per 10^6 yr. But implicit in this result is the assumption that the energy produced by AGB stars comes from burning hydrogen in a shell at the edge of the stellar core, and that the core mass increases continuously with time due to conversion of H to He. However, recall that Figure 11 shows that the core mass for stars with deep envelope convection does not increase continuously with time. In fact, there is essentially no increase in core mass with time because envelope convection eats inward at each shell flash to replenish almost completely the layer that burnt its hydrogen in the preceding quiescent phase. An examination of the thermal pulsing evolution of 5 $M_\odot$ stars (e.g., Fig. 9) shows that these stars initially increase relatively rapidly in luminosity (as do all AGB stars), but that the rate of increase in luminosity slows down continously. Indeed, when the mass-loss rate becomes large enough to cause a significant decrease in envelope mass, upper AGB stars actually evolve down the AGB!

Finally, we note that our most massive models did not encounter the radiation pressure ejection mechanism proposed by Wood & Faulkner (1986), which operates when the luminosity at the base of the convective envelope exceeds the Eddington luminosity there. The radiation pressure associated with the thermal pulses was shown by these authors to be sufficient to eject the remaining stellar envelope for $M_c \gtrsim 0.86\ M_\odot$ and total mass $M \lesssim 2\ M_\odot$. Our models of initial mass 5 $M_\odot$ satisfy these limits during their final shell flashes ($M_c \sim 0.89$, 0.91 and 0.94 $M_\odot$ for $Z = 0.016$, 0.008, and 0.004, respectively), but they managed (with difficulty!) to hold together. The limiting core mass for the radiation pressure mechanism to operate seems to be slightly greater than that estimated by Wood & Faulkner (1986).

3.3. *AGB Tip Luminosities*

A strong test of our adopted mass-loss formalism is to see if the maximum luminosities we predict for AGB stars of various masses agree with the observed maximum luminosities observed in Magellanic Cloud clusters by Frogel, Mould, & Blanco (990). In Table 2 we list for each of the evolutionary sequences the initial mass M_i, the maximum bolometric luminosity [M_{bol}^{max}(EAGB)] during the E-AGB phase, and the maximum and minimum luminosities [M_{bol}^{max}(TPAGB) and M_{bol}^{min}(TPAGB), respectively] of optically visible TP-AGB stars during quiescent evolution. Only the quiescent phase has been considered in order to exclude the brief luminosity excursions associated with shell flashes. Optically visible stars are assumed to be those where the mass-loss rate is less than the radiation-pressure-driven limit (i.e., the superwind rate).

In Figure 19 each of the above luminosities is plotted against initial mass. The thick solid line in Figure 19 shows the maximum luminosity reached by AGB stars in LMC clusters from Frogel et al. (1990). The line is a linear fit through the upper points in their Figure 14 [from (SWB, m_{bol}) = (2, 12.2) to (7, 13.9)], and their SWB type has been converted to initial mass using their Table 3. We have adopted the LMC distance modulus of 18.3 which Frogel et al. (1990) used to derive cluster ages (if a larger distance modulus were adopted, the AGB tips would be more luminous, but there would also be an increase in turnoff mass which would tend to cancel out any change of position in the line representing ABG tip luminosities in the $M_{bol} - M_i$ plane).

From Figure 19, it is clear that for $M_i \lesssim 3.5\ M_\odot$, there is excellent agreement between our estimated tip luminosities and those observed. Since most mass loss occurs during the superwind phase, this result suggests that our adopted superwind mass-loss rates and point of onset for the superwind are realistic. At 5 $M_\odot$, we predict higher luminosities than observed. In fact, the observed luminosities are similar to the maximum E-AGB luminosities at this mass. Given the rapid decrease in AGB lifetime noted above from stars more massive than $\sim 3.5\ M_\odot$, we suspect that the low observed maximum luminosity at these masses is simply due to small sample statistics and that the AGB tip luminosities at high mass are more luminous than the current estimates based on clusters. We certainly know that AGB stars exist with luminosities up to

TABLE 2

PROPERTIES OF AGB STARS

M_i ($M_\odot$)	Z	M_{bol}^{max} (EAGB)	M_{bol}^{min} (TPAGB)	M_{bol}^{max} (TPAGB)	M_{EAGB}^{min} ($M_\odot$)	M_f ($M_\odot$)	P_{max} (days)	t_{opt} (yr)	t_{swind} (yr)	t_{swind}/t_{opt}
1.0	0.016	−3.61	−3.12	−4.03	1.000	0.568	740	4.34E+05	6.1E+04	0.141
1.5	0.016	−3.73	−3.29	−4.52	1.500	0.600	1180	7.29E+04	9.8E+04	0.135
2.0	0.016	−3.78	−3.32	−4.90	2.000	0.633	1510	1.06E+06	1.2E+05	0.114
2.5	0.016	−3.65	−3.02	−5.14	2.500	0.666	1850	2.07E+06	1.1E+05	0.053
3.5	0.016	−5.17	−4.72	−5.65	3.500	0.751	2370	2.97E+05	1.3E+05	0.438
5.0	0.016	−5.91	−5.67	−6.22	5.000	0.891	2800	1.42E+05	1.2E+05	0.843
0.945	0.008	−3.32	−2.90	−3.92	0.722	0.553	375	5.48E+05	2.2E+04	0.040
1.0	0.008	−3.62	−3.07	−4.22	1.000	0.578	620	5.94E+05	5.6E+04	0.094
1.5	0.008	−3.96	−3.29	−4.76	1.500	0.619	970	8.60E+05	7.8E+04	0.091
2.0	0.008	−4.05	−3.37	−5.07	2.000	0.667	1210	1.25E+06	9.1E+04	0.073
2.5	0.008	−3.97	−3.38	−5.32	2.500	0.678	1420	1.72E+06	1.1E+05	0.064
3.5	0.008	−5.44	−5.09	−5.84	3.500	0.794	1900	2.41E+05	1.1E+05	0.457
5.0	0.008	−5.95	−5.75	−6.39	5.000	0.910	2000	2.50E+05	1.1E+05	0.440
0.89	0.004	−3.22	−2.85	−3.98	0.691	0.558	310	7.55E+05	1.6E+04	0.021
1.0	0.004	−3.72	−3.09	−4.46	1.000	0.592	510	8.25E+05	4.3E+04	0.052
1.5	0.004	−3.99	−3.41	−4.91	1.500	0.639	700	9.09E+05	5.8E+04	0.064
2.0	0.004	−3.89	−3.41	−5.24	2.000	0.672	870	1.48E+06	7.6E+04	0.051
2.5	0.004	−4.54	−4.03	−5.46	2.500	0.691	1290	1.15E+06	9.5E+04	0.082
3.5	0.004	−5.70	−5.44	−6.03	3.500	0.853	1100	1.63E+05	8.9E+04	0.545
5.0	0.004	−6.00	−5.86	−6.46	5.000	0.941	1600	2.15E+05	9.7E+04	0.451
1.0	0.001	−3.41	−3.10	−4.68	1.000	0.623	310	1.33E+06	2.7E+04	0.020
1.5	0.001	−3.94	−3.55	−5.05	1.500	0.663	320	1.08E+06	4.7E+04	0.044

$M_{bol} \sim -7$ (Wood et al. 1983). AGB tip luminosities are discussed further in the next section.

3.4. *Visible and Dust-enshrouded Variable Stars*

For at least part of their lifetimes, AGB stars undergo large amplitude, long period variability. This statement applies to AGB stars that have relatively small mass-loss rates and are optically visible (e.g. Mira variables) and to the dust-enshrouded AGB stars that are currently undergoing superwind mass loss (e.g., van Langevelde, van der Heiden, & van Schoonevelde 1990 for Galactic objects; Wood et al. 1992 for LMC objects). The present calculations predict the period range that long period variables (LPVs) on the AGB can have.

In Figure 20 M_{bol} is plotted against the maximum pulsation period P of each helium shell flash cycle (excluding the brief luminosity spike at each flash). For all masses the first point shown corresponds to the first shell flash cycle on the TP-AGB, while successive points on the tracks are at approximately equal intervals of time (being separated by one flash cycle). As the luminosity varies with phase of the flash cycle, stars move up and down the tracks formed by these points. Note that the periods shown are those that each star would have if it was pulsating but no pulsational stability analysis has been performed to see if the stars are actually pulsating.

Initially, the stars evolve steadily up the AGB increasing in luminosity and period until the onset of the superwind, at which point the period increases rapidly. It is clear that the more massive the star, the greater is its acceleration to long periods as the superwind develops. The reason for this is simply that there is more mass to be lost. A larger decrease in T_{eff} and a larger increase in P result due to the combined effects of the lower T_{eff} and the direct mass dependence of P (see eq. [4]). The maximum period reached increases with mass and metallicity (see Table 2).

Also shown in Figure 20 are known optically visible LPVs in the LMC (Hughes & Wood 1990) together with dust-enshrouded LPVs (Wood et al. 1992). For $M \lesssim 2.5\ M_\odot$, the optically visible LPVs generally occupy the region of the theoretical tracks just before onset of the superwind, as expected. However, in the 3.5 and 5 $M_\odot$ cases, the optically visible LPVs are situated in positions corresponding to the early superwind

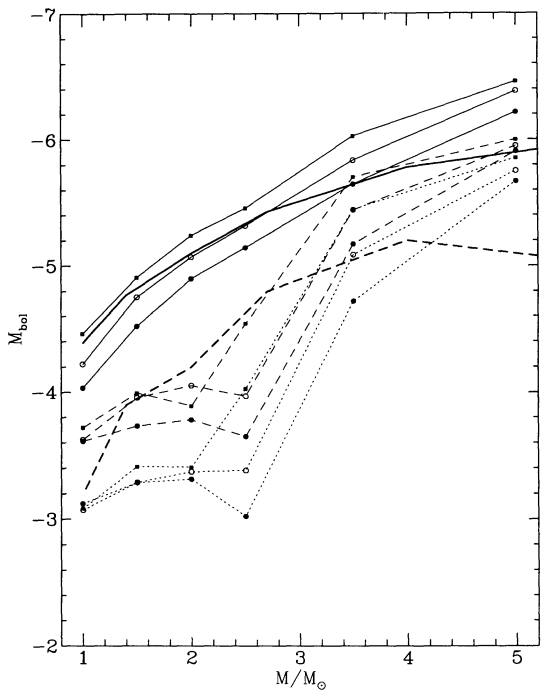

FIG. 19.—The luminosity at the tip of the optically visible AGB (*thin solid lines*), the maximum luminosity on the E-AGB (*thin dashed lines*), and the minimum luminosity on the TP-AGB (*dotted lines*) plotted as a function of the initial mass. Filled circles correspond to $Z = 0.016$, open circles to $Z = 0.008$, and squares to $Z = 0.004$. Also shown is the luminosity at the tip of LMC cluster AGBs (*thick solid line*) and the transition luminosity from M to C stars in LMC clusters (*thick dashed line*), from the data in Frogel et al. (1990).

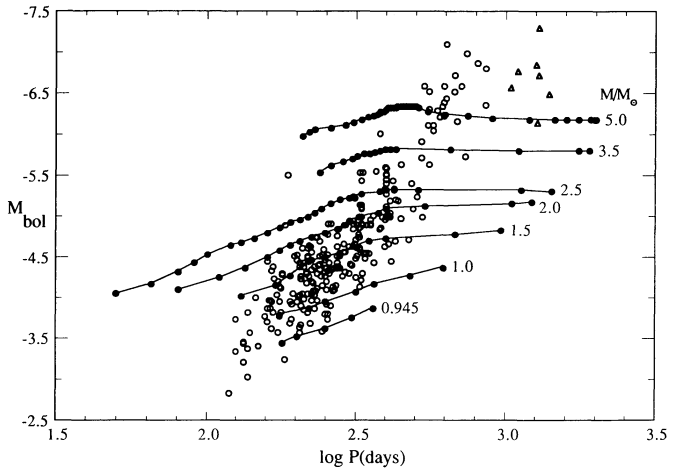

FIG. 20.—M_{bol} plotted against the pulsation period P when P is at its maximum during the quiescent hydrogen burning phase of each shell flash cycle (*solid circles joined by lines*). The initial mass is indicated at the end of each track. Also shown are optically visible LPVs in the LMC (*open circles*) and dust-enshrouded AGB stars in the LMC (*open triangles*).

phases of the models, whereas the superwind clearly has not started in these stars. The reason for this problem is that the periods shown in Figure 20 are calculated using the T_{eff} given by the evolution program whereas the period used in the mass-loss formulae was computed from the T_{eff} given by equation (6). This equation gives T_{eff} values ~ 0.03 cooler than the evolution code for the massive stars. Since $P \propto T_{eff}^{-3.88}$, the value of log P used in the mass-loss formula is ~ 0.12 larger than shown in Figure 20. Use of a better analytic formula for T_{eff} would have given longer periods for the massive optically visible LPVs in Figure 20 and a small increase ($\Delta M_{bol} \sim -0.25$) in the final AGB luminosities for these stars (extrapolating the optically visible sequences in Fig. 20). As noted in the previous section, our estimated AGB tip luminosities are already higher than the observational estimates of Frogel et al. (1990). The existence of the optically visible LPVs at the periods observed suggests that the AGB limits of Frogel et al. (1990) are indeed too faint.

In Table 2 the duration t_{swind} of the superwind phase is given along with the total duration t_{opt} of the optically visible TP-AGB. For the lower mass stars, the superwind phase is $\sim 10\%$ of the TP-AGB lifetime, while for the 3.5 and 5 $M_\odot$ stars the duration of the superwind phase is similar to that of the optically visible phase. The fact that half the massive TP-AGB stars are hidden within dust shells could further help to explain the apparent lack of observed upper AGB stars in the LMC (e.g., Reid & Mould 1985, 1991).

It is clear that the 1.5, 2.0, and 2.5 $M_\odot$ tracks start well before the region where the variable stars are found. This indicates that such stars spend a considerable part of their TP-AGB lifetimes as nonvariables. On the other hand, stars near maximum quiescent luminosity on the TP-AGB cannot explain the LPVs with $P < 180$ days and $M_{bol} > -3.7$ since none of the tracks shown in Figure 20 enter this part of the (M_{bol}, log P) plane. Such LPVs could be low-mass stars a few tenths of a magnitude below quiescent luminosity maximum or stars on the E-AGB.

3.5. *The Initial-Final Mass Relation*

The final core masses M_f at which the sequences depart from the AGB are given in Table 2 and plotted against initial mass M_i in Figure 21. We have taken the core mass to be the final mass, as this mass will be very close to the mass of the remnant white dwarf. At the end of the AGB, some of the stars still have substantial H envelopes which will be lost in the transition to the PN region of the H-R diagram.

Also shown in the figure is the observational calibration of the initial mass-final (i.e., white dwarf) mass relation from Weidemann & Koester (1983) and Weidemann (1987). There is clearly a large amount of scatter in the observational calibration, but our theoretical calibration lies at the upper boundary of the distribution of observational points. In fact, the core mass at the beginning of the TP-AGB phase seems to be in better agreement with the mean observational calibration. It is difficult to account for white dwarf masses this small, at least in the case of single star evolution, since such masses imply the nonexistence of TP-AGB stars, whereas we know such stars (e.g., C stars, S stars) definitely exist. We have noted above that the agreement between the theoretical and observational maximum AGB luminosities in the Magellanic Clouds suggests that our adopted superwind mass-loss rates are close to reality. We therefore believe our theoretical initial-final mass relation for single stars is not seriously compromised by the lack of agreement with the observed initial mass–white dwarf relation.

3.6. *Surface Abundance Changes*

3.6.1. *The First and Second Dredge-Ups*

Between the MS and the end of the AGB, low- to intermediate-mass stars experience three types of dredge-up episode during which material that has undergone nuclear pro-

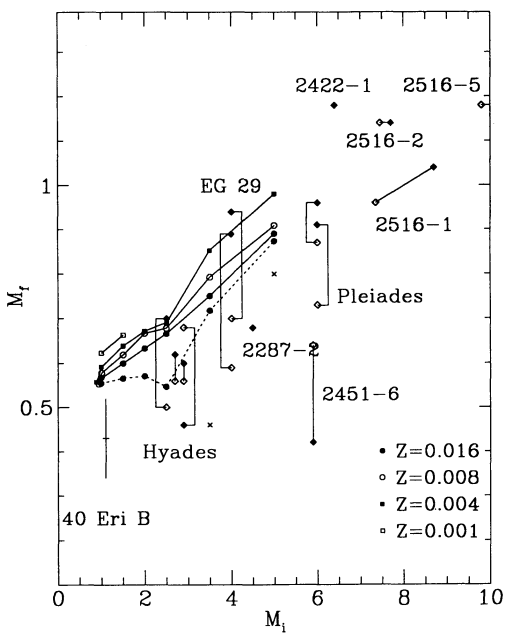

FIG. 21.—Final stellar remnant mass, after AGB mass loss, plotted as a function of the initial mass (*solid curves*). The dashed line represents the core mass at the first helium shell flash for the $Z = 0.016$ calculations. Observational points are taken from Weidemann (1987), and references therein. Annotation of the data points is similar to that presented in Fig. 1 of Weidemann & Koester (1983). Filled diamonds represent masses derived from log g, while open diamonds represent masses derived from the stellar radius. Mass determinations via log g and radius for the same object are joined by a line. The crosses represent the Sanduleak-Pesch binary (Greenstein, Dolez, & Vauclair 1983) where $M_f = 0.8$ was assumed for the primary.

cessing in the stellar interior is mixed to the surface by envelope convection. The first episode takes place on the FGB (Iben 1964), the second during E-AGB evolution (Kippenhahn, Thomas, & Weigert 1965; Weigert 1966), and the third during the TP-AGB phase (Iben 1975; Sugimoto & Nomoto 1975). Products from the CNO cycle are transported to the stellar surface during the first and second dredge-up episodes, while the third dredge-up brings up He shell burning products (^{12}C and *s*-process elements) as well.

Figures 22–23 show surface abundance enhancement factors which result from the first and second dredge-ups. The small ^{4}He enhancements, the ^{12}He enhancements, the ^{12}C depletion by a factor of $\sim$0.7, and the small changes in ^{16}O are consistent with past results (e.g., Becker & Iben 1979; Lattanzio 1986; Sweigert et al. 1989). One noticeable difference between the present calculations and other calculations is the large ^{14}N enhancement factor of up to $\sim$9 for the $Z = 0.004$ case. Becker & Iben (1979) studied the mass range $3 \leq M_i \leq 11$ and found that ^{14}N was only enhanced by a factor of 2.7, at most. The other studies cited above found similar enhancement factors, and, indeed, our solar metallicity case is in agrement with this result. The reason that large enhancement factors were found in the lower metallicity cases studied here is that these mixtures began with N/C ratios of $\frac{1}{2}$ (LMC) or $\frac{1}{4}$ (SMC) solar. Thus, for a given amount of dredged-up CN-cycled material, the N enhancement factor will clearly be greater in the present calculations.

Second dredge-up, which occurs during the early-AGB phase, is significant mostly in models of relatively large mass ($M_i \gtrsim 5\ M_\odot$) where the H-burning shell is dormant (Becker & Iben 1979). Once the base of the convective envelope penetrates the H-He discontinuity during second dredge-up, large enhancements ($\sim$20%) in ^{4}He occur (Becker & Iben 1979). The fact that we saw no such enhancements indicates that our most massive models are, at 5 $M_\odot$, just below the mass limit where significant second dredge-up occurs.

Type I PNs (Peimbert 1978) show enhancements of both N (N/O $\geq$ 1) and He [N(He)/N(H) $\geq$ 0.14 or $X_{\rm He} \geq 0.36$], and they are thought to come from relatively massive AGB stars with $M \gtrsim 2.4\ M_\odot$ (Peimbert & Serrano 1980). The He enhancement in our models with $M \geq 2.5\ M_\odot$ are small by comparison with those in type I PNs. Thus there seems to be a need to make dredge-up go deeper in order to bring up more He at second dredge-up.

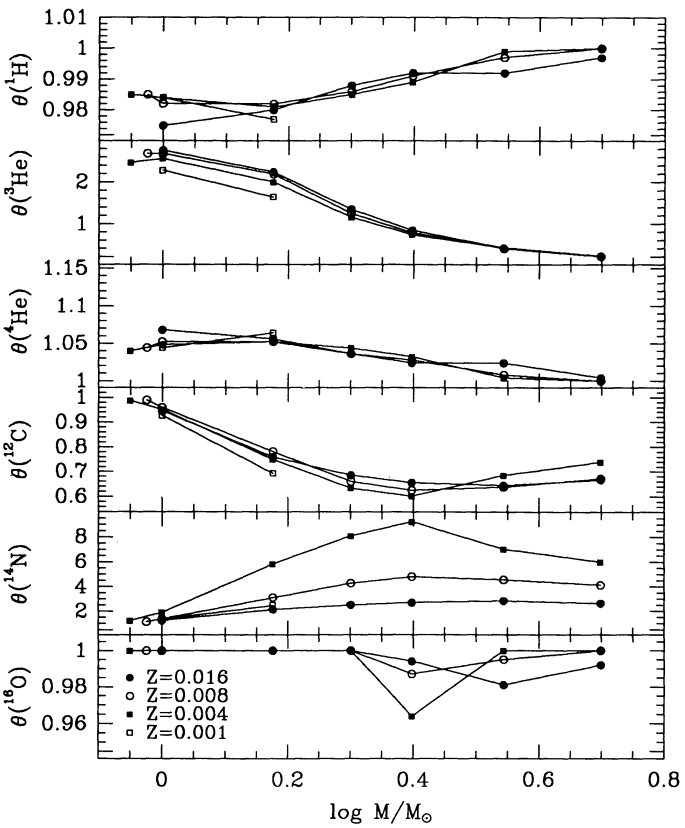

FIG. 22.—Ratio θ of surface abundance after first dredge-up to the initial, main-sequence abundance, except for ^{3}He where $\theta(^3\text{He})$ is 4000 times the ^{3}He abundance (the initial ^{3}He abundance is zero).

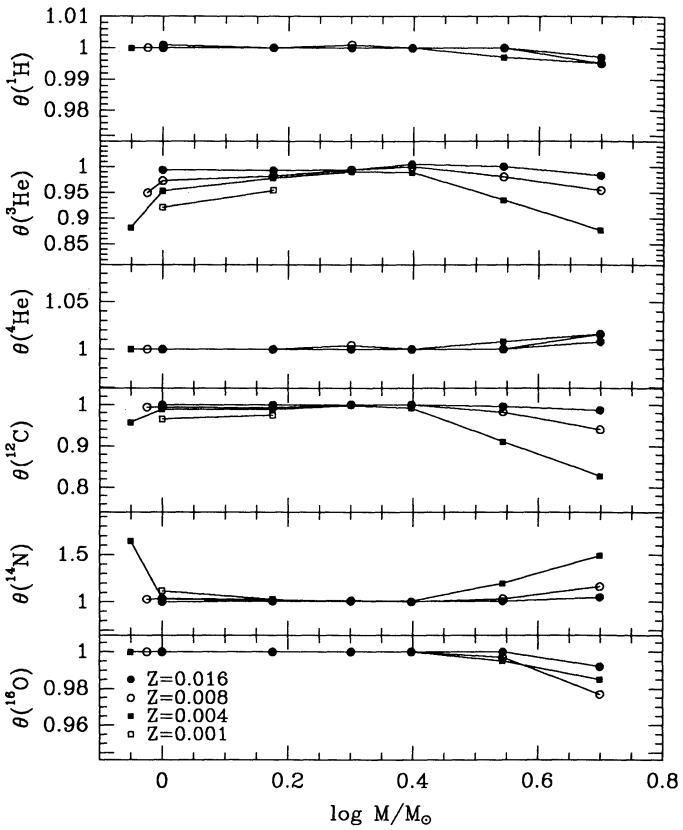

FIG. 23.—Ratio θ of surface abundance after second dredge-up to that after first dredge-up.

3.6.2. *Third Dredge-Up*

The abundances at the end of the TP-AGB phase, relative to those at the beginning of this phase (i.e., at the end of the second dredge-up phase), are plotted in Figure 24. Clearly, some ^{12}C enhancement has occurred due to third dredge-up events at helium shell flashes: if efficient enough, third dredge-up leads to carbon star formation. The amount of ^{12}C enhancement increases strongly with metallicity and mass as found in other studies (e.g., Wood 1981; Lattanzio 1987; Boothroyd & Sackmann 1988d). The metallicity dependence of third dredge-up is supported observationally by the fact that the ratio of C to M stars increase from the Galactic bulge to

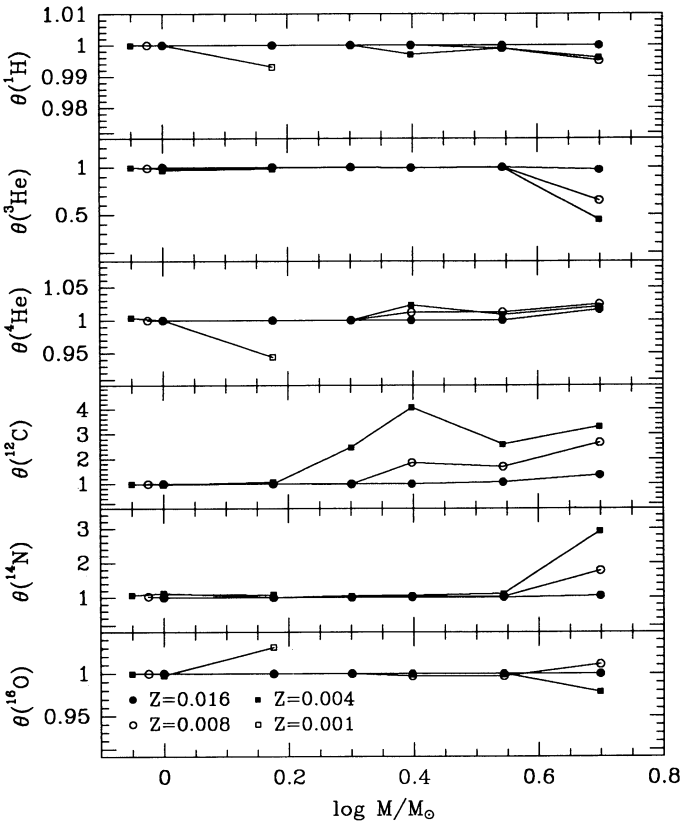

FIG. 24.—Abundances at the end of the TP-AGB relative to the abundances after second dredge-up.

the LMC to the SMC, a sequence of decreasing metallicity (Blanco, Blanco, & McCarthy 1978).

Most stellar evolution calculations fail to predict C stars at the observed luminosities (see Lattanzio 1989a for a review; Westerlund et al. 1991 and Frogel et al. 1990 for recent observations). Where dredge-up has been obtained in the past in stars with a metal abundance appropriate for the Galaxy or Magellanic Clouds (Iben 1975; Wood 1981; Lattanzio 1987, 1989b; Boothroyd & Sackmann 1988d), it has only been when the stellar mass is relatively large ($M \geq 1.5\ M_{\odot}$). Even then, the lowest luminosity carbon stars that result are ~ 0.5 mag brighter than the lowest observed luminosities at masses $\gtrsim 1.5\ M_{\odot}$ (comparing data in Frogel et al. 1990 with results in Lattanzio 1989b).

Two ways of enhancing dredge-up and C star production are (1) to decrease the metal abundance (the last three sets of authors cited above obtained dredge-up at $Z = 0.001$), and (2) to increase the mixing-length parameter α. By using both $Z = 0.001$ and $\alpha = 3$, Boothroyd & Sackmann (1988d) obtained dredge-up in a $0.81\ M_{\odot}$ star at $M_{\rm bol} \sim -3.6$, still brighter than the luminosity of the faintest C stars in old clusters in the SMC and LMC (see Fig. 19 which shows the M-to-C star transition line of Frogel et al. 1990). However, the use of such large values of α is questionable: $\alpha \sim 1.5$ appears to reproduce observed stellar effective temperatures during many stages of evolution prior to the AGB (Castellani et al. 1992; Vandenberg 1991).

We have not been able to reproduce the C star distribution observed in the SMC and LMC. For LMC abundances ($Z = 0.008$), we found dredge-up only for $M_i \geq 2.5\ M_{\odot}$ and only the $5\ M_{\odot}$ star became a carbon star, and then only during the latter parts of the superwind phase when the star would be optically obscured. For the SMC abundances ($Z = 0.004$), we find dredge-up only for $M_i \geq 2.0\ M_{\odot}$ and carbon star formation for $M_i \geq 2.5\ M_{\odot}$ (although the $2\ M_{\odot}$ star develops C/O = 0.94 and nearly becomes a C star). In Figure 19 the thick dashed line indicates the transition luminosity from M to C star in LMC clusters, as given in Table 3 of Frogel et al. (1990). This line indicates that C stars form at the end of the E-AGB almost as soon as shell flashes start (see also Lattanzio 1991). Clearly, all dredge-up calculations need some new physics or additional process to produce the observed C stars. The new, larger OPAL opacities (Rogers & Iglesias 1992) might help, as would envelope undershoot (Alongi et al. 1991).

3.6.3. *Hot-Bottom Burning in Massive AGB Stars*

The other notable abundance change in Figure 24 is a large ^{14}N enhancement in the $5\ M_{\odot}$ stars with SMC and LMC abundance. This is caused by the so-called hot-bottom burning (HBB) (Iben 1973; Sackmann, Smith, & Despain 1974; Scalo, Despain, & Ulrich 1975; Renzini & Voli 1981) during quiescent evolution. Hot-bottom burning occurs when envelope convection cycles envelope material through the upper parts of the H burning shell where ^{12}C is converted to ^{14}N. The enhanced ^{7}Li abundances which have been observed in luminous ($M_{\rm bol} \gtrsim -6$) Magellanic Cloud AGB stars (Smith & Lambert 1989) are attributed to HBB and the berylium transport mechanism (Cameron & Fowler 1971). In this process, ^{7}Be is formed from ^{3}He produced primarily during the main-sequence phase, and ^{7}Be is transported rapidly to cooler regions by convection where ^{7}Li is produced via the reaction $^{7}\mathrm{Be}(\beta^{-}, \gamma)^{7}\mathrm{Li}$. Our calculations do find HBB in luminous AGB stars, but we do not treat the processes involved in detail so we cannot make detailed comparisons with observations. The combined transport and nucleosynthesis processes are best examined in a separate calculation using input from the evolution calculations. Finally, we note that the He and ^{14}N dredged up at each flash (Fig. 11) in the $5\ M_{\odot}$ stars will also contribute to surface abundance enhancements.

4. SUMMARY

The results of stellar evolution calculations from the main sequence through to the end of the AGB phase with mass loss have been presented. The mass-loss rates used are based on empirical determinations for AGB stars. It is shown that typical low-mass AGB stars naturally suffer one or more superwind phases of mass loss toward the end of the AGB, these superwinds occurring during the latter parts of the quiescent phases of helium shell flash cycles. The mass-loss rates produced by the superwind are similar to those required for PN production, and the occurrence of multiple superwind phases can account for the existence of AGB stars with hollow shells and multiple shell PNs. Each superwind phase leads to the loss of a few tenths of a solar mass. A comparison of the maximum AGB luminosities predicted by the models of initial mass $M_i \lesssim 3\ M_{\odot}$ with the maximum luminosities reached by Magellanic Cloud stars shows excellent agreement between theory and observation and suggests that the adopted empirical mass-loss rates can be used to realistically model AGB evolution. For the more massive stars, the predicted maximum AGB luminosities are greater than current observational esti-

mates from Magellanic Cloud clusters, but evidence is presented that these estimates are too faint. The initial mass-final mass relation resulting from our calculations predicts white dwarf masses $\sim 0.1\ M_{\odot}$ larger, at a given initial mass, than those in current observational calibrations of the initial mass-white dwarf mass relation.

REFERENCES

Alongi, M., Bertelli, G., Bressan, A., & Chiosi, C. 1991, The Formation and Evolution of Star Clusters, ed. Kenneth Janes (ASP Conf. Ser. 13), 223
Andersen, J., Nordström, B., & Clausen, J. V. 1990, ApJ, 363, L33
Becker, S. A., & Iben, I., Jr. 1979, ApJ, 232, 831
———. 1980, ApJ, 237, 111
Bertelli, G., Bressan, A. G., Chiosi, C., & Angerer, K. 1985, A&AS, 66, 191
Bessell, M. S., Brett, J. M., Scholz, M., & Wood, P. R. 1989, A&AS, 77, 1
Blanco, B. M., Blanco, V. M., & McCarthy, M. F. 1978, Nature, 271, 638
Blöcker, T., & Schönberner, D. 1991, A&A, 244, L43
Boothroyd, A. I., & Sackmann, I.-J. 1988a, ApJ, 328, 632
———. 1988b, ApJ, 328, 641
———. 1988c, ApJ, 328, 653
———. 1988d, ApJ, 328, 671
———. 1992, ApJ, 393, L21
Boroson, T. A., & Liebert, J. 1989, ApJ, 339, 844
Bowen, G. 1988, ApJ, 329, 844
Buzzoni, A., Fusi-Pecci, F., Buonanno, R., & Corsi, C. E. 1983, A&A, 128, 94
Cameron, A. G. W., & Fowler, W. A. 1971, ApJ, 164, 111
Caputo, F., Castellani, V., Chieffi, A., Pulone, L., & Tornambeè, A. 1989, ApJ, 340, 241
Caputo, F., Martinez Roger, C., & Paez, E. 1987, A&A, 183, 228
Castellani, V., Chieffi, A., Pulone, L., & Tornambè, A. 1985, ApJ, 296, 204
Castellani, V., Chieffi, A., & Straniero, O. 1992, ApJS, 78, 517 (CCS)
Castellani, V., Giannone, P., & Renzini, A. 1971, Ap&SS, 10, 360
Castor, J. I. 1981, in Physical Processes in Red Giants, ed. I. Iben & A. Renzini (Dordrecht: Reidel), 285
Caughlan, G. R., & Fowler, W. A. 1988, Atomic Data Nucl. Data, 40, 283
Caughlan, G. R., Fowler, W., Harris, M., & Zimmerman, B. 1985, Atomic Data Nucl. Data, 32, 197
Chan, S. J., & Kwok, S. 1988, ApJ, 334, 362
Chiosi, C., Bertelli, G., & Bressan, A. 1987, in Late Stages of Stellar Evolution, ed. S. Kwok & S. R. Pottasch (Dordrecht: Reidel), 213
Chu, Y.-H., Jacoby, G. H., & Arendt, R. 1987, ApJS, 64, 529
Cox, A. N., & Stewart, J. N. 1970a, ApJS, 19, 243
———. 1970b, ApJS, 19, 261
Cox, J. P., & Giuli, R. T. 1968, Principles of Stellar Structure, Vol. 1 (New York: Gordon & Breach)
Dufour, R. J. 1984, in IAU Symp. 108, Structure & Evolution of the Magellanic Clouds, ed. S. van den Bergh & K. S. de Boer (Dordrecht: Reidel), 353
Eder, J., Lewis, B. M., & Terzian, Y. 1988, ApJS, 66, 183
Fowler, W. A., Caughlan, G. R., & Zimmermann, B. A. 1975, ARA&A, 13, 69
Frank, A., Balick, B., & van der Veen, W. 1992, in IAU Symp. 155, Planetary Nebulae, ed. R. Weinberger & A. Acker (Dordrecht: Kluwer), in press
Frogel, J. A., Mould, J., & Blanco, V. M. 1990, ApJ, 352, 96
Fusi Pecci, F., & Renzini, A. 1976, A&A, 46, 447
———. 1978, in The HR Diagram, ed. A. G. D. Philip & D. S. Hayes (Dordrecht: Reidel), 225
Gezari, D. Y., Schmitz, M., & Mead, J. M. 1984, Catalog of Infrared Observations (NASA Reference Publication 1118)
Greenstein, J. L., Dolez, N., & Vauclair, G. 1983, A&A, 127, 25
Härm, R., & Schwarzschild, M. 1975, ApJ, 200, 324
Harris, M. J., Fowler, W. A., Caughlan, G. R., & Zimmermann, B. A. 1983, ARA&A, 21, 165
Hearn, A. G. 1990, in From Miras to Planetary Nebulae: Which Path for Stellar Evolution?, ed. M. O. Mennessier & A. Omont (Yvette Cedex: Éditions Frontières), 121
Heske, A. 1990, A&A, 229, 494
Heske, A., Forveille, T., Omont, A., van der Veen, W. E. C. J., & Habing, H. J. 1990, A&A, 239, 173
Hollowell, D., & Iben, I. Jr. 1988, ApJ, 333, L25
Holzer, T. E., & MacGregor, K. B. 1985, in Mass Loss from Red Giants, ed. M. Morris & B. Zuckerman (Dordrecht: Reidel), 229
Huebner, W. F., Merts, A. L., Magee, N. H. Jr., & Argo, M. F. 1977, Astrophysical Opacity Library (Los Alamos Scientific Laboratory, LA-6760-M)
Hughes, S. M. G., & Wood, P. R. 1990, AJ, 99, 784
Iben, I. Jr. 1964, ApJ, 140, 1631
———. 1973, ApJ, 185, 209
———. 1975, ApJ, 196, 525
———. 1977, ApJ, 217, 788
Iben, I. Jr., & Renzini, A. 1983, ARA&A, 21, 271
Jura, M. 1987, ApJ, 313, 743
———. 1990, in From Miras to Planetary Nebulae: Which Path for Stellar Evolution?, ed. M. O. Mennessier & A. Omont (Yvette Cedex: Éditions Frontières), 67
Kaler, J. B. 1974, AJ, 79, 594
Kippenhahn, R., Thomas, H.-C., & Weigert, A. 1965, Z. Ap., 61, 241
Knapp, G. R. 1985, ApJ, 293, 273
Knapp, G. R. 1986, ApJ, 311, 731
Knapp, G. R., & Morris, M. 1985, ApJ, 292, 640
Knapp, G. R., et al. 1989, ApJ, 336, 822
Lattanzio, J. C. 1986, ApJ, 311, 708
———. 1987, ApJ, 313, L15
———. 1989a, in Evolution of Peculiar Red Giants, ed. H. R. Johnson, & B. Zuckerman (Cambridge: Cambridge Univ. Press), 161
———. 1989b, ApJ, 344, L25
———. 1991, ApJS, 76, 215
Lèfevre, J. 1989, A&A, 219, 265
Lloyd Evans, T. 1976, MNRAS, 174, 169
Maeder, A. 1975, A&A, 40, 303
Margulis, M., Van Blerkom, D. J., Snell, R. L., & Kleinmann, S. G. 1990, ApJ, 361, 673
Meatheringham, S. J., & Dopita, M. A. 1991a, ApJS, 75, 407
———. 1991b, ApJS, 76, 1085
Monk, D. J., Barlow, M. J., & Clegg, R. E. S. 1988, MNRAS, 234, 583
Olofsson, H., Carlstrom, E., Eriksson, K., & Gustaffson, B. 1992, A&A, 253, L17
Olofsson, H., Eriksson, K., & Gustaffson, B. 1988, A&A, 196, L1
Paczyński, B. 1970, A&A, 6, 426
Paczyński, B., & Ziolkowski, J. 1968, Acta Astron., 18, 255
Peimbert, M. 1978, in IAU Symp. 76, Planetary Nebulae: Observations and Theory, ed. Y. Terzian (Dordrecht: Reidel), 215
Peimbert, M., & Serrano, A. 1980, Rev. Mexicana Astron. Af., 5, 9
Pottasch, S. R. 1984, Planetary Nebulae (Dordrecht: Reidel), 31
Reid, N., & Mould, J. R. 1985, ApJ, 299, 236
———. 1991, in IAU Symp. 148, The Magellanic Clouds, ed. R. Haynes & D. Milne (Dordrecht: Kluwer), 363
Reimers, D. 1975, in Problems in Stellar Atmospheres and Envelopes, ed. B. Bascheck, W. H. Kegel, & G. Traving (Berlin: Springer), 229
Renzini, A. 1981, in Physical Processes in Red Giants, ed. I. Iben Jr. & A. Renzini (Dordrecht: Reidel), 431
Renzini, A., & Fusi Pecci, F. 1988, ARA&A, 26, 199
Renzini, A., & Voli, M. 1981, A&A, 94, 175
Rogers, F. J., & Iglesias, C. A. 1992, ApJS, 79, 507
Ross, J. E., & Aller, L. H. 1976, Science, 191, 1223
Roxburgh, I. W. 1967, Nature, 215, 838
Russell, S. C., & Bessell, M. S. 1989, ApJS, 70, 865
Russell, S. C., & Dopita, M. A. 1990, ApJS, 74, 93
Sackmann, I.-J., Smith, R. L., & Despain, K. H. 1974, ApJ, 187, 555
Scalo, J. M., Despain, K. H., & Ulrich, R. K. 1975, ApJ, 196, 805
Schild, H. 1989, MNRAS, 240, 63
Schönberner, D. 1979, A&A, 79, 108
———. 1981, A&A, 103, 119
———. 1983, ApJ, 272, 708
Seidel, E., Demarque, P., & Weinberg, D. 1987, ApJS, 63, 917
Simon, N. 1992, ApJ, 387, 162
Smith, V. V., & Lambert, D. L. 1989, ApJ, 345, L75
Steigman, G. 1983, in Primordial Helium, ed. P. A. Shaver, D. Kunth, & K. Kjär (Garching: ESO), 13
Sugimoto, D., & Nomoto, K. 1975, PASJ, 27, 197
Sweigert, A. V. 1987, ApJS, 65, 95
Sweigert, A. V., & Demarque, P. 1972, A&A, 20, 445
Sweigert, A. V., Greggio, L., & Renzini, A. 1989, ApJS, 69, 911
———. 1990, ApJ, 364, 527
Sweigert, A. V., & Gross, P. G. 1976, ApJS, 32, 367
Tuchman, Y. 1991, ApJ, 383, 779
VandenBerg, D. A. 1991, in The Formation & Evolution of Star Clusters, ed. Kenneth Janes (ASP Conf. Proc. 13), 183
VandenBerg, D. A., & Laskarides, P. G. 1987, ApJS, 64, 103
van Langevelde, H. J., van der Heiden, R., & van Schoonevelde, C. 1990, A&A, 239, 193
Vassiliadis, E., Dopita, M. A., Morgan, D. H., & Bell, J. F. 1992, ApJS, 83, 87
Wagoner, R. V. 1973, ApJ, 179, 343
Wannier, P. G., & Sahai, R. 1986, ApJ, 311, 335
Weidemann, V. 1987, A&A, 188, 74
———. 1990, ARA&A, 28, 103
Weidemann, V., & Koester, D. 1983, A&A, 121, 77
Weigert, A. 1966, Z. Ap., 64, 395
Westerlund, B. E., Azzopardi, M., Breysacher, J., & Rebeirot, E. 1991, A&AS, 91, 425
Whitelock, P., Feast, M., & Catchpole, R. 1991, MNRAS, 248, 276
Willems, F. J., & de Jong, T. 1986, ApJ, 309, L39
Willson, L. A., in Pulsations in Classical & Cataclysmic Variables, ed. J. P. Cox & C. J. Hansen (Boulder: JILA), 284
Wood, P. R. 1974, ApJ, 190, 609

Wood, P. R. 1979, ApJ, 227, 220
———. 1981, in Physical Processes in Red Giants, ed. I. Iben & A. Renzini (Dordrecht: Reidel), 135
———. 1986, in Stellar Pulsation, ed. A. N. Cox, W. M. Sparkes, & S. G. Starrfield (Berlin: Springer), 250
———. 1990a, in From Miras to Planetary Nebulae: Which Path for Stellar Evolution?, ed. M. O. Mennessier & A. Omont (Yvette Cedex: Éditions Frontières), 67
———. 1990b, in Confrontation Between Stellar Pulsation and Evolution, ed. C. Cacciari & G. Clementini (ASP Conf. Ser. 11), 355
Wood, P. R., & Bessell, M. S. 1983, ApJ, 265, 748
Wood, P. R., Bessell, M. S., & Fox, M. W. 1983, ApJ, 272, 99
Wood, P. R., Bessell, M. S., & Paltoglou, G. 1985, ApJ, 290, 477
Wood, P. R., & Cahn, J. H. 1977, ApJ, 211, 499
Wood, P. R., & Faulkner, D. J. 1986, ApJ, 307, 659
———. 1987, Proc. Astron. Soc. Australia, 7, 75
Wood, P. R., Whiteoak, J. B., Hughes, S. M. G., Bessell, M. S., Gardner, F. F., & Hyland, A. R. 1992, ApJ, 397, 552
Wood, P. R., & Zarro, D. M. 1981, ApJ, 247, 247
Zijlstra, A. A., Loup, C., Waters, L. B. F. M., & de Jong, T. 1992, A&A, 265, L5
Zuckerman, B., & Dyck, H. M. 1986, ApJ, 311, 345
Zuckerman, B., Dyck, H. M., & Claussen, M. J. 1986, ApJ, 304, 401